Effects of microencapsulated phase change materials on chloride ion transport properties of geopolymers incorporating slag and, metakaolin, and cement-based mortars

Bouha El Moustapha, Stéphanie Bonnet, Abdelhafid Khelidj, Nicolas Maranzana, Daniel Froelich, Abderahmane Khalifa, Isselmou Ahmedou Babah

Effects of microencapsulated phase change materials on chloride ion transport properties of geopolymers incorporating slag and, metakaolin, and cement-based mortars

Bouha El Moustapha [a,b,c,d,*], Stephanie Bonnet [c], Abdelhafid Khelidj [c], Nicolas Maranzana [a], Daniel Froelich [a], Abderahmane Khalifa [e], Isselmou Ahmedou Babah [d]

[a] Arts et Métiers Institute of Technology, LCPI, HESAM Université, F-75013, Paris, France
[b] Aix Marseille University, CNRS, IUT Aix Marseille University, LMA UMR 7031, F-13453, Marseille, CEDEX 13, France
[c] Nantes Université, Ecole Centrale Nantes, CNRS, GeM, UMR 6183, 44600 Saint Nazaire, France
[d] University of Nouakchott AL-Aasriya, Faculty of Sciences and Techniques/UCME, BP 880, Nouakchott, Mauritania
[e] MAGMA Group Laboratory (www.magma-groupe.com), Villa 051 Bis, BP 2942, Nouakchott, Mauritania

ARTICLE INFO

Keywords:
Geopolymer
Microencapsulated phase change materials
Durability
Chloride diffusion
Resistivity
Porosimetry

ABSTRACT

The addition of microencapsulated phase change materials (MPCMs) to geopolymers is a technological alternative for meeting the thermal comfort and energy efficiency requirements of buildings. However, current research is limited to the effects of MPCM addition on mechanical and thermal performances of geopolymers. New MPCM applications, therefore, require additional research on durability indicators (chloride diffusivity, porosity, absorption, etc.).

The objective of this research is to examine the effects of MPCM addition on sodium chloride ion transport properties of geopolymer mortars based on a combination of blast furnace slag and metakaolin, and Portland cement based mortars. Twelve different mortars (three cement-based and nine geopolymer-based) are studied by varying the MPCM content (0%, 5% and 10%, respectively) within two types of mortar: a geopolymer mortar (GPM) and a cement mortar (CM). With this aim in view, a series of characterizations are conducted, including determination of total porosity by water saturation, analysis of pore structure distribution by mercury intrusion porosimetry (MIP), measurement of electrical resistivity, capillary water uptake, stationary-state migration coefficient "D_{ss}" and non-stationary-state migration coefficient "D_{nss}", and determination of chloride ion binding capacity.

The results show that MPCM addition increases total porosity, which in turn increases capillary water absorption and decreases GPM and CM electrical resistivity. Conversely, MPCM addition also reduces critical diameter and pore connectivity, due of the agglomeration effect. MPCMs also increase chloride ion binding capacity. Both effects results in decreased stationary state migration coefficient. Finally, the study shows that the chemical reaction of GPM with chloride ions delays chloride penetration in stationary state conditions. However, the same is not true for the non-stationary state method. This demonstrates the technical limitations of this method for the characterization of GPM in comparison to CM.

* Corresponding author. 1 Arts et Métiers Institute of Technology, LCPI, HESAM Université, F-75013, Paris, France.
E-mail address: Bouha.el_moustapha@ensam.eu (B. El Moustapha).

https://doi.org/10.1016/j.jobe.2023.106887

Nomenclature

MPCM	Microencapsulated Phase Change Materials
GBFS	Granulated Blast furnace Slag
MK	Metakaolin
GPM	Geopolymer mortar
CM	Cement mortar
D_{ss}	Stationary state migration coefficient
D_{nss}	Non- Stationary state migration coefficient

1. Introduction

Energy-efficient buildings design is a key concern for researchers, as the sector accounts for 36% of global energy consumption and 40% of the global greenhouse gas emissions [1]. CO_2 emissions are responsible for three-quarters of these emissions. The production of building materials and the energy required to maintain adequate thermal comfort in buildings alone account for the majority of CO_2 emissions associated with the building sector [2].

In this context, microencapsulated phase change materials (MPCMs) have attracted scientific attention because of their high capacity to store thermal energy in buildings. MPCM use of reduces energy demand and contributes to the improvement of thermal comfort. MPCMs can store a large amount of energy in the form of latent heat during phase change at an ambient temperature close to human comfort requirements. They prevent heat from entering buildings during peak hours; storing it during the day and releasing it at night [3].

However, for practical application, MPCMs need be incorporated into building materials like concrete, plaster and/or gypsum. Ordinary Portland Concrete (OPC) is the most widely used in the construction industry [4]. OPC exhibits a large volume and surface area exposed to the indoor and outdoor environments of the buildings, large thermal energy storage capacity and high mechanical strength. Therefore, this material is a promising candidate for MPCM use, as highlighted in the study by Ren et al. [5], where a 10% MPCM addition significantly improved the storage performance of a high-performance OPC. The maximum surface temperature of this concrete material decreased by 3.9 °C compared to the reference concrete material (without MPCM). Rathore et al. [6] conducted a comprehensive review of the scientific literature (actual laboratory and field tests) over the last thirty years on the use of MPCM to improve building thermal performances. The study concludes that MPCM is compatible with a wide range of building materials such as perforated brick, concrete, cement, gypsum and plasterboard to improve thermal energy storage of buildings. Similar results are observed by Drissi et al. [7], who report that MPCM use can reduce the annual energy consumption by about 50% to maintain the desired thermal comfort [7].

The production of Portland cement has a significant impact on the environment because of its high energy and natural resource consumption. It is also responsible for greenhouse gas emissions, particularly carbon dioxide, accounting for 7% of total CO_2 emissions [8]. To reduce this environmental impact, geopolymer binders can be used as an alternative to Portland cement to produce sustainable and low carbon emission concrete materials [9]. Geopolymers are produced by mixing an alkaline solution with a reactive aluminosilicate powder such as metakaolin (MK), fly ash (FA) or granulated blast furnace slag (GBFS), which are considered industrial by-products or clays. The use of geopolymers instead of Portland cement could reduce CO_2 emissions and the amount of waste produced by the construction sector. According to Davidovits et al. [10], CO_2 emissions associated with the production of geopolymers are reduced by 70–80% compared with Portland cement. Moreover, geopolymer concrete properties, including high compressive strength [10], good resistance to sulfate and acid attack [11], and high fire resistance [12], are similar to, if not higher than those of OPC.

In order to produce a geopolymer with improved mechanical and durability properties, it has been found that the combination of CASH (calcium silicate and alumina hydrate) and NASH (sodium silicate and alumina hydrate) gels has potential for property enhancement [13]. A geopolymer mixture including GBFS and a small amount of silica (SiO_2) and alumina (Al_2O_3) rich MK contributes to a better workability and a structure mainly composed of the above mentioned coexisting gels.

Nevertheless, the addition of MPCM in a geopolymer matrix to develop geopolymer-MPCM concrete materials with improved thermal and mechanical performances could be an interesting issue to address the reduction of CO_2 emissions related to energy use in buildings and Portland cement production. According to Shadnia et al. [14] MPCMs reduce the internal temperature of geopolymer cells by up to 4.5–5.5 °C. Cao et al. [15] conclude that MPCMs can decrease the internal temperature of a geopolymer concrete wall by about 3 °C and reduce energy consumption by 25% while maintaining inside temperature at 23 °C. El Moustapha et al. [16], in a previous study, have examined the effects of the combination of CASH and NASH gels on the thermal properties of a geopolymer-MPCM based on GBFS and MK. Their findings show that the thermal capacity reaches 1280 J/kg.K, a value higher than the thermal capacity of Portland cement-based mortars. In a recent study by Fang et al. [17], thermocouples are placed in some geopolymer-PCM pastes to measure temperature change with time. The results show that PCM addition results in a significant drop in the temperature (up to 10.5 °C) compared to the geopolymer samples without PCM. Muraleedharan and Yashida Nadir [18] propose a literature review of studies investigating PCM addition to geopolymers. This survey shows that geopolymers can be used as a potential material for PCM addition, in appropriate amounts, as substitutes for fine aggregates to improve building thermal performances. It also underlines that PCM addition to geopolymer materials is more cost-effective and environmentally friendly than when added to

conventional materials.

However, the above studies are limited to the investigation of the thermal and mechanical properties of the material. Although the technology is rapidly developing and attracts academic attention, a survey of the literature reveals that little research has been devoted to MPCM impact on geopolymer durability. No previous study has been conducted to investigate chloride ion penetration.

It is also important to note that, according to the IUCN (International Union for Conservation of Nature), more than 60% of the world population currently lives in extended coastal zones. Population projections for 2035 anticipate that this figure will rise to over 75% [19]. This perspective suggests that many future buildings in these areas will be at risk of destruction over time due to chloride ingress.

The deterioration of reinforced concrete due to chloride ingress is an extensively studied factor of concrete durability. Chlorides penetrate by ionic diffusion, capillary absorption and by convection in response to liquid pressure gradients. They initiate rebar corrosion through depassivation of the embedded reinforcement, reducing concrete load-bearing capacity and potentially degrading the concrete structure [20]. A number of published studies investigating geopolymers without MPCM show that geopolymers have comparable [21] or even higher [22] resistance to chloride penetration than OPC. Some other studies focus on chloride penetration measurements using the Rapid Chloride Permeation Test (RCPT), ASTM C1202/AASHTO T277. This method is commonly used to assess OPC resistance to chloride penetration [23]. This method is based on the observation of concrete electrical conductivity, which is dependent on the chemistry of the pore solution, which in turn significantly affects measurements in alkali-activated materials. A high alkali concentration of in the geopolymer pore solution leads to high electrical conductivity measurement results. This is explained by the high content of Na^+ and other cations found in the geopolymer pore solution. These alkali cation loads are also recorded during testing and interfere with the final results [24]. Bernal et al. [25] conclude that this method cannot be considered a reliable indicator of the determination of geopolymer resistance to chloride penetration.

Direct measurement of chloride flux through the material as a diffusion indicator, rather than through the transmitted charge is, therefore, more relevant. The accelerated migration methods (stationary state and non-stationary state) developed by Andrade et al. [26], Truc et al. [27] and Tang et al. [28] are reliable for calculating the chloride migration coefficient. Unlike the RCPT method, which takes into account concrete electrical conductivity measurements, these tests are used to measure chloride ion concentration that has migrated into concrete by accelerating chloride transport with an electric field applied to the sample tested. Chloride flux measurements in the samples allow, on the one hand, for the calculation of the migration coefficient (D_{ss}) in stationary state conditions, and, on the other hand, for the determination of the average chloride penetration depth (X_d) using silver nitrate, as an indicator to calculate the migration coefficient (D_{nss}) in non-stationary state conditions. These coefficients are linked together by the material porosity and chloride ion binding capacity [29].

In order to analyze D_{ss} and D_{nss} migration coefficient results, the solid matrix and chloride ion interactions must be quantified. A good knowledge of these ionic interactions is an essential step in the determination of chloride transport in concrete. Chlorides, indeed, can be found in the concrete matrix in two different forms: chemically- or physically-bound chloride, and free chloride, which moves freely within the concrete pore solution. The ratio of free to bound chlorides is called the chloride binding capacity [30]. Free chlorides initiate corrosion of reinforced concrete by providing the electrolyte for electrochemical reactions and the electron flow released in the anodic zone [31]. Consequently, the chloride binding capacity of cementitious materials is an important parameter for predicting reinforced concrete structure service life [32]. However, while it is still necessary to improve our knowledge of the chloride binding capacity of geopolymer-based materials [31], no published study has yet been conducted to address the effects of MPCM addition on chloride binding capacity in cementitious and geopolymer-based materials.

However, concrete resistivity measurement is a method providing good information on material pore connectivity and pore network tortuosity. Both are factors that can affect penetration of aggressive ions into concrete. Electrical resistivity is defined as a volumetric property that indicates material ability to conduct electrical charges [33]. The study of this property applied to geopolymer and MPCM-based materials has not yet been documented.

The objective of this research is to examine the effects of MPCM addition to Portland cement-based mortars (CM) and geopolymer mortars (GPM), based on a combination of GBFS and MK, on durability indicators related to corrosion risk. The sub-objectives of this research are twofold:

1. To evaluate chloride penetration properties of geopolymer-MPCM in both stationary and non-stationary state conditions.
2. To study the effects of CASH and NASH gel coexistence on geopolymer-MPCM durability indicators.

Different indicators related to corrosion risk as mentioned in Ref. [29] are investigated (total porosity by water saturation and pore structure distribution analysis by mercury intrusion porosimetry (MIP) device, electrical resistivity measurement, capillary water absorption measurement, migration coefficient measurements in stationary state condition 'D_{ss}' and non-stationary state 'D_{nss}' condition, and chloride ion binding capacity measurement).

2. Experimental procedure

2.1. Materials

The GPM studied here is a mixture of GBFS, MK, an alkaline solution (mixture of sodium silicate and sodium hydroxide), standardized sand (CEN NF 196–1) and water. CM is a mixture of cement (CEM II/B-M class 32.5 R) [34], standardized sand (CEN NF 196) and water.

GBFS has been supplied by ECOCEM, France, and MK by KENZAI (ecological materials), France. The cement used is produced by EQIOM Ciments, France.

The chemical compositions and physical properties of CEM II, GGBS and MK are summarized in Table 1.

According to Table 1, GBFS is composed of SiO_2 and Al_2O_3 for a total of 48%, and 43% CaO. Regarding MK, SiO_2 and Al_2O_3 contents are high (total: 96%).

GBFS has a density of 2900 kg/m^3 and a d_{50} of 13.25 μm, while MK has a density of 2400 kg/m^3 and a d_{50} of 7.13 μm, respectively. CEM II has a density of 3030 kg/m^3 and a d_{50} of 8.47 μm. MPCM has a density of 840 kg/m^3 and an average particle size of 22.1 μm. Finally, standardized sand has a density of 2400 kg/m^3. In addition, the specific surface areas of GBFS, MK, CEM II, and MPCM are 0.37, 17; 0.44, and 0.12 m^2/g, respectively.

The activating solution is a mixture of sodium silicate and sodium hydroxide. According to the supplier, sodium silicate is composed of 27.53% SiO_2, 11.47% Na_2O and 61% H_2O. The sodium hydroxide NaOH is a caustic soda with a purity of 98%. Both solutions and standardized sand are supplied by the French company E2EM.

The MPCM studied here consists of white spherical microcapsules by Microteck laboratory, United States, known by the technical name Nextek 28 D. The microcapsule is made of two parts: a polymer wall and a core material (kerosene). The composition is ≥ 97% kerosene powder. The polymer is a urea polymer, cross-linked with a modified low molecular weight polyethylene. MPCM melting temperature is 28 °C and heat capacity is between 180 and 190 (J/g). MPCM general properties of, based on the manufacturer's data sheet, are presented in Table 2.

2.2. Mixture proportions

Twelve different formulations are studied: three based on standardized MC and nine based on GPM. For both types of mortar, W/C ratio and sand-to-binder ratio are set at 0.5 and 3, respectively, considering that the geopolymer binder (cement equivalent) corresponds to the sum of GBFS, MK and the solid part of the alkaline solution. For this reason, the mass ratio (GBFS + MK)/SA is set at 3, with SA corresponding to the solid part of the alkaline solution, according to the recommendations by Hasnaoui et al. [35].

MK replaces part of the GBFS in the geopolymer matrix with a substitution rate of 0%, 10% and 20%, respectively. The mass ratio of sodium silicate (SS) to sodium hydroxide (SS/NaOH) is set at 2.5, according to the study of Bernal et al. [13].

The sodium hydroxide solution is prepared with a concentration of 12 M, mixed with sodium silicate and cooled for 24 h before mixing. More information on the design process of geopolymer-MPCM mortars is provided in a previous study [16].

MPCM contents of 0%, 5%, and 10%, respectively, are chosen for both types of mortar (cement-based and geopolymer). For MPCM inclusion, the sand substitution approach is chosen. This is the most commonly used method in this field. Moreover, according to a study conducted by Pilehvar et al. [36], MPCM inclusion causes the minimum deterioration in mechanical performances.

CM and GPM mix proportions are listed in Table 3 according to the percentages chosen. The first three formulations are based on standardized CM, the last nine on GPM.

The amount of water contained in the two alkaline solutions is taken into account s that the W/binder ratio is equal to 0.5.

Standard NF 196–1 [37] is followed for the production of standardized CM, chosen as a reference for comparison with geopolymer-based mortars. This standard specifies the method for the determination of compressive strength and, optionally, flexural strength of cement mortars. However, there is currently no specific standard for the preparation of geopolymers. This has led us to follow a mixing method described in the literature [38]. To obtain a homogeneous paste, GBFS and MK are first mixed with the alkaline solution and water for 90 s. Sand is then added and mixed for 5 min. Finally, MPCM is added and mixed for 2 min.

Mortars are cast in different types of molds (cylindrical and prismatic). Prismatic molds have dimensions of 40 × 40 × 160 mm^3. They are used for the electrical resistivity test. Cylindrical molds with dimensions (D = 63 mm; H = 130 mm) and (D = 40 mm; H = 100 mm) are used to measure total porosity by water saturation, D_{ss} and D_{nss} coefficients, chloride ion binding capacity and water absorption by capillarity.

After casting, the molds are stored in an air-conditioned room (temperature 20 ± 1 °C and relative humidity 50 ± 5%) for 24 h before demolding. Finally, 1.5-cm^3 samples are taken from the core of the mortars after they have been cured for 28 days. They are used to measure pore structure distribution using MIP.

2.3. Experimental procedure and methods

2.3.1. Experimental procedure

In this study, all the experimental tests have been performed at room temperature, i.e., between 19 °C and 21 °C. All tests, including

Table 1
Chemical composition and physical properties of CEM II, GBFS and MK.

Chemical composition (%)	CEM II	GBFS	MK
SiO_2	7.47	37.30	55.0
Al_2O_3	2.18	10.70	41.0
Fe_2O_3	2.84	0.20	1.2
CaO	69.02	43.00	0.1
MgO	–	6.50	0.2
TiO_2	–	0.70	0.4
$(Na_2O + K_2O)$eq	–	0.80	1.8
Specific gravity	303	2.90	2.4
Blaine specific surface Area (m^2/g)	0.37	0.44	17.0
Average grain size (μm)	8.47	13.25	7.13

Table 2
General properties of MPCM (manufacturer's information).

Appearance	White to slightly off-white color
Form	Dry powder (≥97% solids)
Core material	Paraffin
Particle size (mean)	14-24 μm
Melting point	28 °C (82.4 °F)
Melting temperature	180–190 J/g
Specific gravity (g/cm^3)	0.84
Temperature stability	Extremely stable - less than 1% leakage when heated to 250 °C
Thermal cycling	Multiple

Table 3
CM and GPM formulations (kg/m^3) [16].

	Mixtures proportions (kg/m^3)								
Sample	Cement	GGBS	MK	Sand	MPCM	Na_2SiO_3	NaOH	GPM water	CM water
$CM_{0/0/0}$	585.9	–	–	1757.8	–	–	–	–	293.0
$CM_{0/0/5}$	585.9	–	–	1673.8	28.4	–	–	–	293.0
$CM_{0/0/10}$	585.9	–	–	1582.0	56.8	–	–	–	293.0
$GPM_{100/0/0}$	–	439.5	–	1757.8	–	267.9	127.7	42.6	–
$GPM_{100/0/5}$	–	439.5	–	1673.8	28.4	267.9	127.7	42.6	–
$GPM_{100/0/10}$	–	439.5	–	1582.0	56.8	267.9	127.7	42.6	–
$GPM_{90/10/0}$	–	395.5	43.9	1757.8	–	267.9	127.7	42.6	–
$GPM_{90/10/5}$	–	395.5	43.9	1673.8	28.4	267.9	127.7	42.6	–
$GPM_{90/10/10}$	–	395.5	43.9	1582.0	56.8	267.9	127.7	42.6	–
$GPM_{80/20/0}$	–	351.6	87.9	1757.8	–	267.9	127.7	42.6	–
$GPM_{80/20/5}$	–	351.6	87.9	1673.8	28.4	267.9	127.7	42.6	–
$GPM_{80/20/10}$	–	351.6	87.9	1582.0	56.8	267.9	127.7	42.6	–

mortar curing time, are presented in Fig. 1.

2.3.2. *Water porosity and mercury instrusion porosimetry (MIP)*

Water porosity is determined in accordance with NF P 18–459 [39] after 28 days of curing. MIP is a relevant technique that to

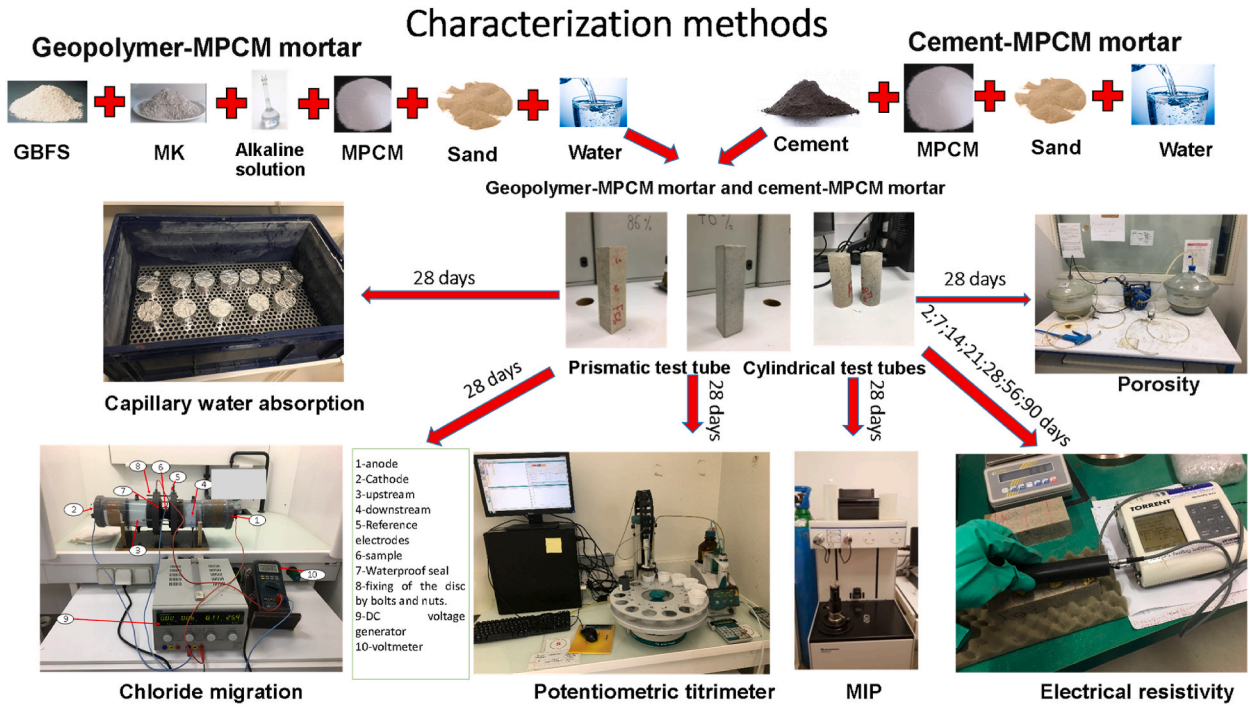

Fig. 1. The different stages of the experimental study.

characterize pore size distribution in cementitious materials [40]. This method consists in injecting mercury (a non-wetting fluid with a contact angle greater than 90°) into the pores of the sample with increasing pressure. As the pressure rises, mercury is forced into increasingly smaller pore spaces. Pressure required to force mercury into a pore is inversely proportional to pore size. Washburn's equation (1) describes the relationship between pressure and capillary diameter as:

$$D = \frac{-4\gamma \cos\varnothing}{p} \tag{1}$$

where "D" is the diameter of an analogous cylindrical pore that must be filled at pressure "p" to be filled, 'γ' is the mercury surface tension, and 'Ø' is the mercury-pore wall contact angle. The mercury contact angle used for pore size calculation is 130°. The surface tension is 0.485 N/m. The size of the samples studied is given in Section 2.2. Prior to MIP testing, the samples are stored in an oven at 60 °C until their mass stabilizes. The experimental device used in this study is called "AutoPore IV 9500". It can apply pressures up to 400 MPa.

2.3.3. *Capillary water absorption*

Measurements of water absorption by capillarity are carried out in accordance with standard NF EN 13057 [41]. The samples tested are cylinders with a diameter of 63 mm and a height of 40 mm. They are dried at a temperature of 60 °C until the mass stabilizes. After drying, the samples are coated with aluminum as shown in Fig. 1 and stored at 20 °C and 50% RH for 24 h prior to testing. The aluminum coating reduces water evaporation during testing. The samples are weighed 'M_0' and submerged in water in the container to a depth of ±2 mm. At each time interval, the samples are removed from the container, wiped with a damp sponge, weighed 'M_x', and returned to the container. Measurement intervals are 15 min, 30 min, 1 h, 2 h, 4 h, 8 h and 24 h.

The capillary absorption coefficient at each time point x is defined by the relationship given in Equation (2) as:

$$C_{a,x} = \frac{M_x - M_0}{A} \tag{2}$$

where 'M_x' is the mass of the sample at a given time, expressed in g, 'M_0' is the mass of the sample after drying and coating with aluminum and 'A' is the sample cross-section (m^2).

2.3.4. *Electrical resistivity*

In this study, electrical resistivity is measured using a non-destructive method. The device used is called 'Wenner resistivimeter' [42]. It consists of 4 electrodes aligned at a constant distance (a) equal to 5 cm. The principle consists in applying an electric current 'I' between the two external electrodes. The electrical potential between them is then measured. The electrical resistivity is calculated by the control acquisition unit, according to Equation (3), where 'ρ' is the resistivity (Ω × m), 'a' is electrode spacing (m), 'V' is the voltage (volts), and 'I' is the intensity of the current injected into the sample. We obtain:

$$\rho = 2\pi a \frac{V}{I} \tag{3}$$

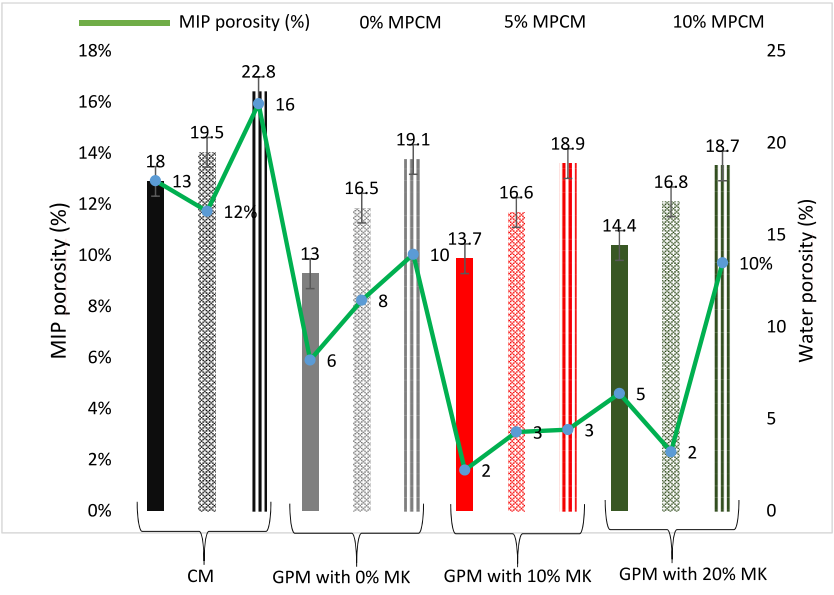

Fig. 2. CM and GPM total porosity (water saturation and MIP).

2.3.5. Chloride equilibrium and transport properties

2.3.5.1. Chloride binding isotherms. The method of Tang and Nilsson [30] is used to determine the chloride ion interaction isotherms in both types of mortar. This method is based on the determination of the amount of ions that are bound at equilibrium by samples submerged in solutions of different concentrations. A set of 28-day-old samples is ground to a size between 0.25 and 2 mm. These samples are then dried for three days at 40 °C using silica gel until constant weight is reached.

A mass of 50 g is placed in a solution of 200 ml containing chloride ions (NaCl) at concentrations of 0.05 M, 0.25 M, 0.5 M and 1 M. In order to imitate the high alkalinity of the geopolymer interstitial solution, this solution is prepared at a concentration of 1.0 M NaOH. The flasks are stored at a temperature of 20 ± 2 °C for two months until equilibrium is reached.

Chloride content is determined by potentiometric titration with silver nitrate $AgNO_3$ (0.05 M). The amount of bound chloride ions C_b (mg/g) can be calculated according to the equilibrium method, based on the reduction of the initial chloride concentration, using Equation (4) as:

$$c_b = \frac{M_{Cl} V (c_0 - c_f)}{m} \tag{4}$$

where 'M_{Cl}' is the molar mass of the chloride (g/mol), 'V' is the volume of the solution in ml; 'C_0' is the initial chloride concentration of the solution (mol/l); 'C_f' is the chloride concentration at equilibrium (mol/l); 'm' is the dry mass of the sample in g.

2.3.5.2. Stationary state migration test. Chloride migration tests are carried out in accordance with standard XP-P18-461 [43]. The samples are cut 40 mm thick and sealed in epoxy to promote unidirectional chloride ion flow of during the test period. The samples are then saturated with a NaOH solution (0.1 mol/l) under vacuum for 48 h. After saturation, each sample is placed between the two compartments of a cell (Fig. 1) sealed using flat circular silicon seals. Both compartments are filled with a basic NaOH solution of 4 g/l (0.1 mo/l). The upstream compartment contains a NaCl solution loaded at a concentration of 30 g/l (0.5 mo/l), close to that of sea water.

The tests are carried out at a temperature of 20 ± 2 °C with a voltage of 25 V applied between the sample faces. Chloride concentration in the downstream compartment is determined by potentiometric titration, and by adding silver nitrate AgNO3 (0.05 M) to an acidic medium. A Methrom 736 titrator coupled to an autosampler is used for the titration. The system is controlled using Methrom TiNET2 software.

The coefficient of chloride migration in stationary state conditions 'D_{ss}' (m^2/s) can be calculated from Equation (5) in the form:

$$D_{ss} = \frac{RTL}{ZFEc_0} J \tag{5}$$

where 'J' is the chloride ion flux (mol/m^2.s), 'z' is the valence of the ion equal to 1, 'F' is the Faraday constant (96,480 J/(V. mol)), 'E' is the measured electric field (V/m), 'L' is the thickness of the sample (0.04 m), 'R' is the perfect gas constant (8.314 J/(mol.K)), 'T' is the absolute temperature (293.15 ± 2K), 'Co' is the chloride concentration in the upstream compartment (0.5 mol/m3).

2.3.5.3. Non-stationary state migration test. The non-stationary migration test is carried out in accordance with standard XP-P18-462 [44] or NT BUID 492 [45]. Procedures for sample preparation, vacuum saturation, and concentration of the two solutions in both cell compartments are similar to those of the stationary state migration test. An electric field of 28.5 V is applied between the sample faces for the migration of the chloride ions from the upstream compartment to the downstream compartment. The test consists in measuring the average chloride penetration depth 'X_d' into the test body, determined by spraying a solution of $AgNO_3$.

Colorimetric testing reveals the chloride penetration front on each of the two split surfaces. The silver nitrate solution reveals the interface between the chloride-free zone (darker) and the chloride-contaminated zone (lighter) by color contrast. The interface is visible about 20–30 min after spraying. The depth (corresponding to the distance in mm between the external test body surface and the penetration front) is measured at 4 points on the two fracture surfaces obtained after splitting using a caliper.

The coefficient of migration in the non-stationary state conditions 'D_{nss}' (m^2/s) appears in Fick's second law of diffusion. It is calculated using Equation (6) as:

$$D_{nss} = \frac{RTe}{ZF\Delta E} \cdot \frac{X_d - \alpha\sqrt{X_d}}{\Delta t} \tag{6}$$

where 'R' is the perfect gas constant equal to 8.314 J.K-1mol-1, 'T' is the absolute temperature (293.15 ± 2K), 'e' is the sample thickness, 'Z' is the chloride ion valence equal to 1, 'F' is the Faraday constant equal to 96,487 J. V-1.mol-1, 'ΔE' is the potential difference across the test body (V), 'X_d' is the average chloride ion penetration depth (m), 'Δt' is the test duration (s). The auxiliary term 'α' is given by Equation (7) as:

$$\alpha = 2\sqrt{\frac{RTe}{ZF\Delta E}} \cdot erf^{-1}\left(1 - 2\frac{c_d}{c_s}\right) \tag{7}$$

where c_s is assumed to be equal to the chloride concentration of the upstream compartment solution ($c_0 = 0.5$ mol.l-1), and c_d is the free chloride concentration in X_d (assumed to be 0.070 mol l^{-1} according to Tang [46]). The term $erf^{-1}\left(1 - 2\frac{c_d}{c_s}\right)$ is equal to 0.764, for c0 = 0.5 mol/l.

3. Results and discussion

3.1. Water porosity and MIP measurements

Total water porosity and MIP measurements are shown in Fig. 2. Clearly, total water porosity results are higher than those obtained using the MIP method. This is due to the fact that the pores of the gel absorb water and swell during saturation process, which can increase the measured values, as pointed out by Aligizak et al. [47]. This phenomenon has also been reported by Borges et al. [48] for GBFS- and MK-based geopolymers.

GPM without MPCM has lower total porosity values in comparison to CM. The good workability of GPM compared with CM could explain these lower values, as shown in a previous study [16]. Furthermore, Yang et al. [49] report similar observations and point out that the improved workability of the geopolymer decreases its porosity.

However, MPCM addition affects the geopolymer total water porosity (without MK) more than CM. These analyses are consistent with the property results (compressive strength and Young's modulus) presented by El Moustapha et al. [16] and the total porosity measured (Fig. 2). These results show that MPCM has a greater effect on GPM without MK, with a reduction in compressive strength of 29.2 MPa and an increase in porosity of approximately 6.2%, after addition of 10% MPCM, whereas compressive strength is reduced by approximately 7 MPa and porosity increased by approximately 4.9% after addition of 10% MPCM in CM [16]. This effect proves that the connection between MPCM and the geopolymer matrix is weak, and that MPCM can create a greater number of air voids in the geopolymer matrix without MK than in the cementitious matrix. These voids may result from the agglomeration of MPCMs during mixing because they are smaller than sand. The agglomeration specific surface area is then much greater than that of sand. This may lead to an amount of paste being adsorbed on the surface, creating voids and increasing porosity during matrix curing, and/or the agglomeration induced may repel or trap water, increasing the water need to cover the entire surface of the particles. Because the water content is kept constant for all the samples, a larger water adsorption surface area of the microcapsules, in comparison with that of sand, creates voids and thus increases the porosity of the mortars studied. This agglomeration can also reduce the density of the transition zone at the paste/MPCM interface and thus increase porosity. The problem of MPCM agglomeration during mixing is discussed by Cao et al. [50] and Hunger et al. [51].

Fig. 3 presents CM and GPM pore size distributions. Overall, the size of the GPM pores is greater than CM, indicating a macroporous structure. Most pores are between 1.6 -20 and 0.02–0.29 μm for GPM and CM, respectively.

The reasons that may explain the difference in pore size between GPM and CM are.

i) Water in the geopolymer is not directly included into the geopolymerization process and therefore much of it remains as pore water and is subject to evaporation, usually causing significant cracking [52].
ii) The geopolymer is affected by oven drying conditions [53]. In their study, Ismail et al. [54] show that CASH gel dries and porosity increases even at very low temperatures. As a result, Zhang et al. [53] conclude that the existing oven-drying methods for the

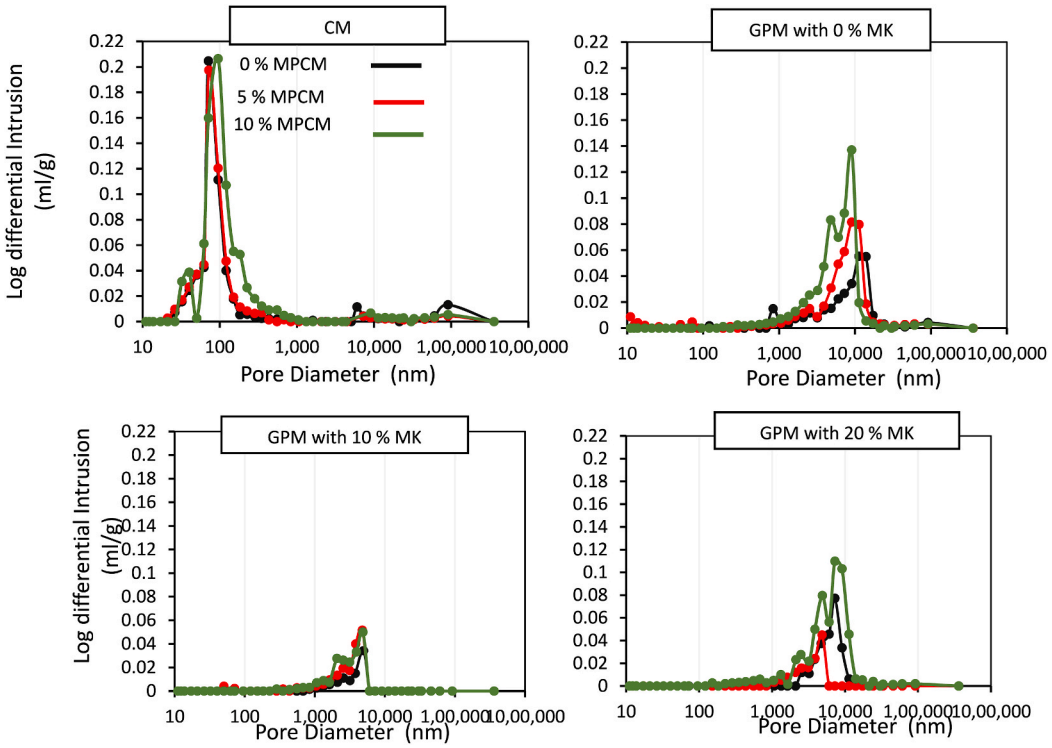

Fig. 3. Pore size distribution for A: (CM), B: (GPM with 0% MK); C: (GPM with 10% MK); D: (GPM with 20% MK). Curing time: 28 days; drying temperature: 60 °C.

evaluation of the durability properties of cementitious materials are not relevant for geopolymers. However, Matalkah et al. [52] state that, due to its structural complexity at nanoscale, CASH gel is not yet fully understood.

Fig. 4 shows the effect of MPCM addition on the critical diameter "dcr". The critical diameter corresponds to the steepest slope of the cumulative pore volume curve. It represents the most commonly measured pore size in the interconnected pores, which allows for maximum percolation through the entire pore system, controlling material transmissivity [47].

MPCM addition shows a decrease in dcr values for GPM and a small increase for CM. For GPM without MK addition, the addition of 5 and 10% of MPCM reduces the dcr value from 11,320 to 9058.1 and 9059.3 nm, respectively. A significant decrease is also observed for all the GPMs after the addition of MK. The GPM with 10% MPCM and 10% MK exhibits a value of 4860 nm. According to Pipilikaki et al. [55], the decrease in dcr values leads to a decrease in pore interconnections. This may explain that, despite the increase in total porosity after MPCM, addition in GPM, MPCM significantly affects the filling of large pores created during drying. This is not true for CM.

As pointed out by Wei et al. [56], pore filling, here, increases the tortuosity of the transport paths. Fig. 5 presents a geopolymer mortar with 10% MPCM. It clearly confirms MPCM agglomeration after curing. MPCM agglomeration, moreover, seems to produce a matrix with a more uniform pore distribution (closed pore distributions), which also explains the reduced "dcr" values.

Fig. 3 shows the effects of MK addition on GPM pore size distribution. Note that GPM pore size decreases when MK is added. This is generally associated with the combination of CASH and NASH gels, which cause the densification and the enhancement of the geopolymer microstructure, reducing pore interconnections. This is in good agreement with the total porosity measured using the MIP method and the dcr values shown in Figs. 2 and 4. Indeed, Bernal et al. [13] and Huseien et al. [57] report the advantage of the good reactivity of MK. Furthermore, the high Si content observed promotes the filling of the studied matrix pores as underlined by Ibrahim et al. [58]. The addition of MK also increases Si content as shown by the EDS analyses conducted in a previous study [16]. This is due to the small particle size and large specific surface area of MK compared to GBFS. This allows for an accelerated reactivity [35] of MK compared to GBFS. As shown in a previous study [16], the large amount of Al_2O_3 and SiO_2 in MK dissolved in the activation medium studied allows for the good dissolution of silica and aluminum in MK. Both effects result in improved geopolymerization through formation of CASH and NASH gels. This observation agrees well with the improvements in compressive strength and Young's modulus achieved after MK addition in a previous study [16].

3.2. *Capillary water absorption*

The total amount of water absorbed by samples of the two types of mortar (cement-based and geopolymer) during a 24-h immersion is displayed in Fig. 6 (A). The CM sample with 0% MPCM shows a total water absorption of about 6.7 (kg/m^2). This value is similar to that found in the study by Mobili et al. [59] for a standard mortar.

It is observed that water absorption capacity of CM is higher than that of GPM. As shown in Fig. 2, this is due to its higher total porosity compared with GPM. Generally, an increase in total porosity results in an increase in total water absorption [59].

Fig. 6 (B) shows an almost linear correlation between water absorption and total porosity results from the present study (CM and GPM) and from the studies conducted by Mobili et al. [[59] and Ismail et al. [54] on geopolymer mortars.

The values measured here are consistent with those found in the published studies. However, some variations in the geopolymer design parameters presented in the following studies may account for the small difference between the results. For example, Ismail et al. [54] have used an E/binder ratio of 0.4, different from the ratio used in this study. Mobili et al. [59]also use a fly ash/metakaolin

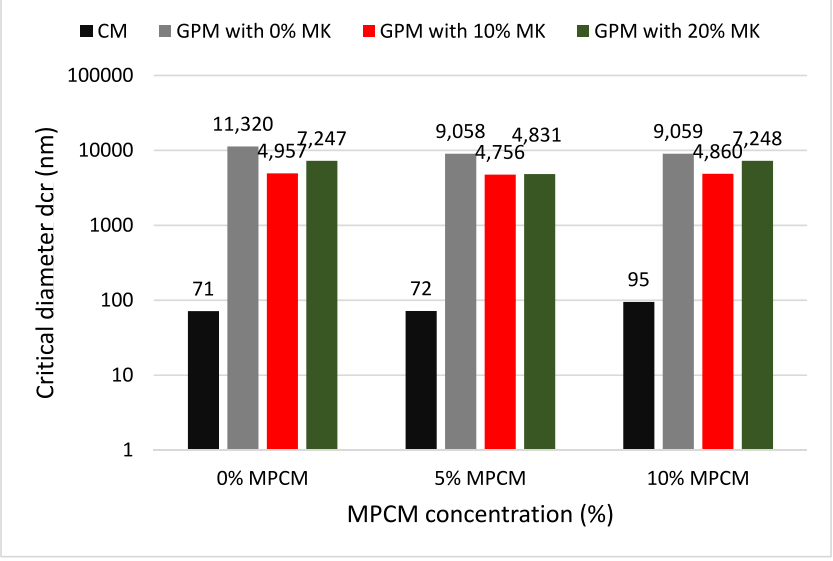

Fig. 4. CM and GPM critical diameter "dcr" using MIP measurements; Curing time: 28 days; drying temperature: 60 °C.

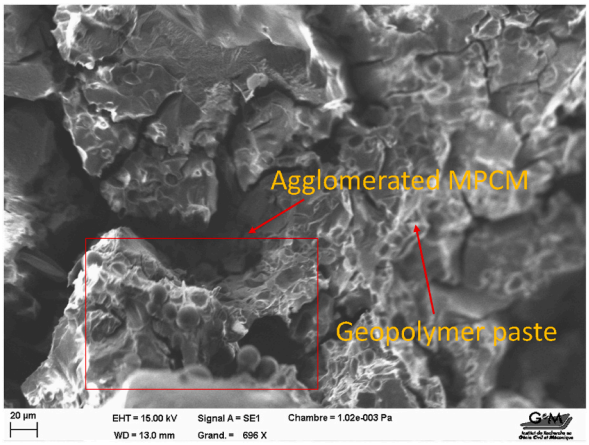

Fig. 5. SEM image illustrating MPCM agglomerations in the geopolymer matrix.

geopolymer with different activation solutions. Geopolymer porosity depends on the W/binder ratio, the ratio of raw materials (slag and/or fly ash/metakaolin), on the geopolymer matrix chemical structure and, especially, on the molar ratio of the activation solution. Porosity results from the combination of air bubbles and microcracks formed in the geopolymer matrix as well as at the paste/sand interfaces, where the quality of the paste/sand interface essentially depends on the fineness of raw materials, the amount of water in the mixture and the characteristics of the activation solution [35].

It must be noted that MPCM addition also leads to an increase in both of these properties (water absorption and total porosity). This observation is confirmed by the total porosity results obtained by the MIP measurements presented in Section 3.1 (Fig. 2). It is attributed to MPCM agglomeration during mixing.

As discussed above, this agglomeration can reduce the density of the transition zone at the paste/MPCM interface. According to Pereira et al. [60], some capillary water absorption phenomena take place in this interface area.

A small increase in the capillary water absorption is observed with the addition of MK. It should be recalled that a constant W/binder is used here. Obviously, the ratio of GBFS to MK is the main factor that determines capillary water absorption properties of GPMs. This is due to NASH gels being more porous than CASH gels after MK addition of [54]. However, the high tortuosity of CASH gel in comparison to NASH gel reduces capillary water absorption, even after the drying protocol that increases pore size [54], as described in Section 3.1.

3.3. Electrical resistivity

Fig. 7 displays the electrical resistivity measurements of the two mortars as a function of curing time (2, 7, 14, 21, 28 and 90 days). The resistivity values after 90 days are between 48 and 210 kΩ cm. Table 4 presents reinforcement corrosion risks as a function of concrete electrical resistivity, quoted by ACI 222 committee [63]. According to this table, reinforcement corrosion risk for both types of mortar is negligible (>20 kΩ cm). Zainal et al. [62] and Ameri et al. [63] underline a negligible risk of corrosion in fly ash-based geopolymer pastes activated using an alkaline solution similar to the one used in the present study.

Measuring the electrical resistivity of concrete materials gives information about pore connectivity and pore network tortuosity. High resistivity corresponds to a material with fewer interconnected pores and a more tortuous pore network. This hinders ion passage through the porous structure of the material [33]. In addition, corrosion risk can be estimated as shown in Ref. [61].

However, GPM has low electrical resistivity between 2 and 28 days compared to CM. This may be due to the low solubility of Ca $(OH)_2$ compared to the Na^+ ions in GPM [63,64]. In fact, the presence of a large number of Na^+ ion conductors from the alkaline activator in the interstitial solution may increase the number of connections in the electrical network and therefore significantly reduce electrical resistivity of geopolymers. GPM resistivity continues to evolve after 28 days, which can generally be attributed to two causes: a continuous evolution of the microstructure (decrease in porosity) or a change in the ionic composition of the interstitial solution as a result of the ionic exchanges between the solid matrix and the pore solution. However, the Young's modulus results obtained in a previous study [16] stabilizes after 28 days of curing. This indicates that the resistivity continuous increase may be caused by an evolution of the pore solution (ionic depletion), in particular with a lower amount of OH^- ions. OH^- ions, indeed, are highly mobile.

The high mobility of Na^+ ions in geopolymer pore solutions makes interpretation of the impact of MPCM addition on resistivity difficult before 28 days. However, between 28 and 90 days after this time (ionic depletion of the solution), MPCM addition of reduces GPM resistivity compared with CM. This is similar to the effect of MPCM addition on total porosity and capillary water absoption described in Sections 3.1 and **3.2,** and probably due to the weakness of the connection between MPCM and the geopolymer matrix, resulting in increased voids and hence reduced electrical resistivity.

Finally, MK addition also seems to improved electrical resistivity. As explained in the previous section, this is due to the coexistence of CASH and NASH gels. According to Ameri et al. [63], the high reactivity of MK, with its ultrafine particles and very high specific surface area, leads to the formation of 3D Si–O–Al polymeric chains (CASH and NASH gel chains). These chains are key factors influencing GPM pore structure and leading to pore refinement, as shown in Section 3.1**,** and thus improving electrical resistivity.

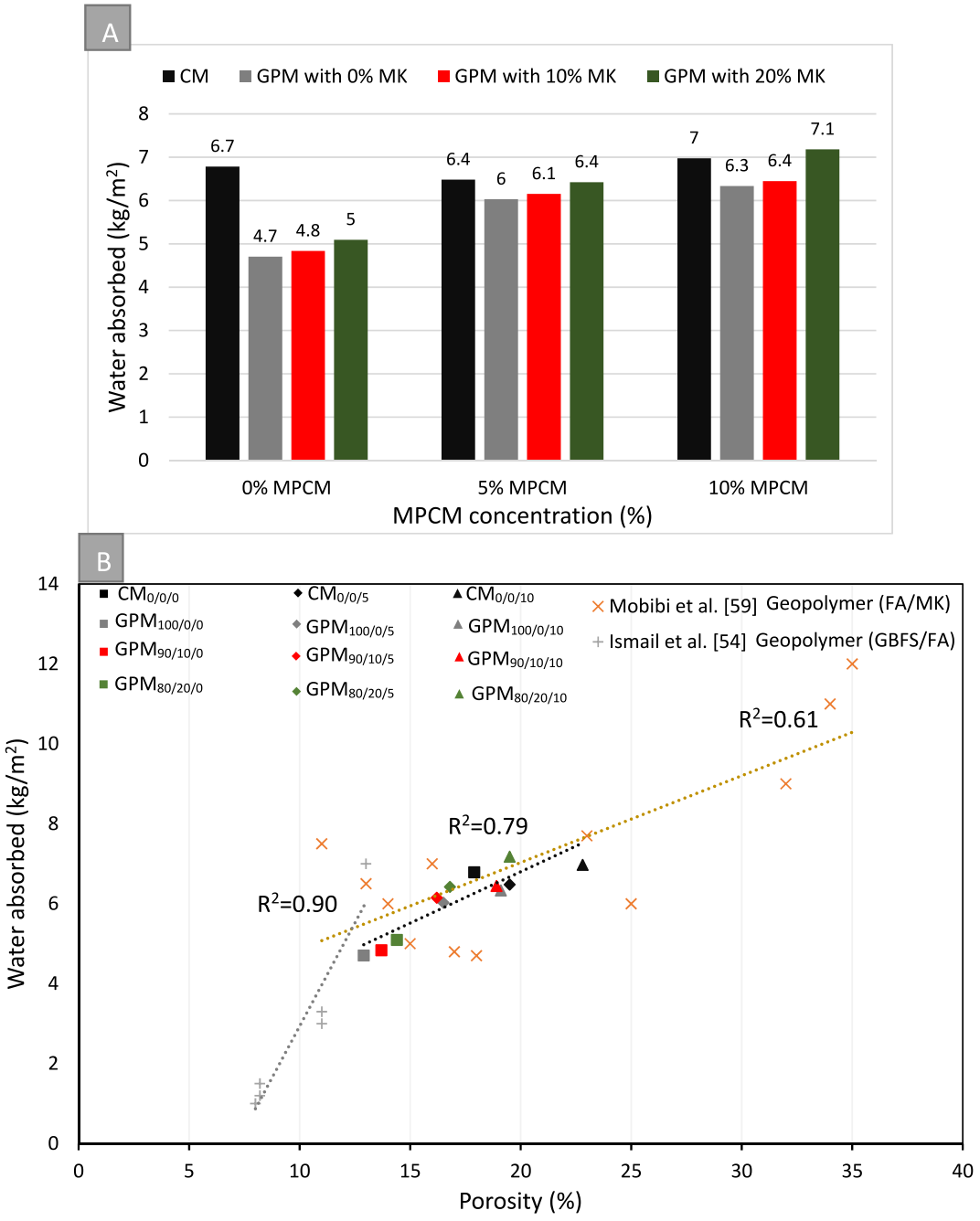

Fig. 6. (A): Capillary water absorption after a curing period of 28 days; ((B): correlation between water absorption by capillary and total water porosity after 28 days of curing/comparison with the studies reported by Mobili et al. [59] Ismail el al [54].

3.4. Chloride equilibrium and transport properties

3.4.1. Chloride binding isotherms

Fig. 8 (A) shows the relationship between free and total bound chloride concentrations (physically and chemically) for GPM and CM with 0 and 10% MPCM. Fig. 8 (B) shows the chloride binding isotherms at 1 mol/l chloride versus MPCM concentration. Fig. 8 (C) shows the chloride binding isotherms from this study compared to studies by Fu et al. [65] and Zhang et al. [66] on geopolymer and by Thomas et al. [67] and Tang et al. [30] on OPC.

Results in Fig. 8 (A) show that an increase in free chloride concentration leads to an increase in the chloride binding capacity. There are two types of chloride binding in cement materials [30]: a physical binding, where chloride adsorption occurs on the hydration products (CSH gel) and a chemical binding, where the AFm phases (alumina, ferric oxide, monosulfate) react with chloride to form

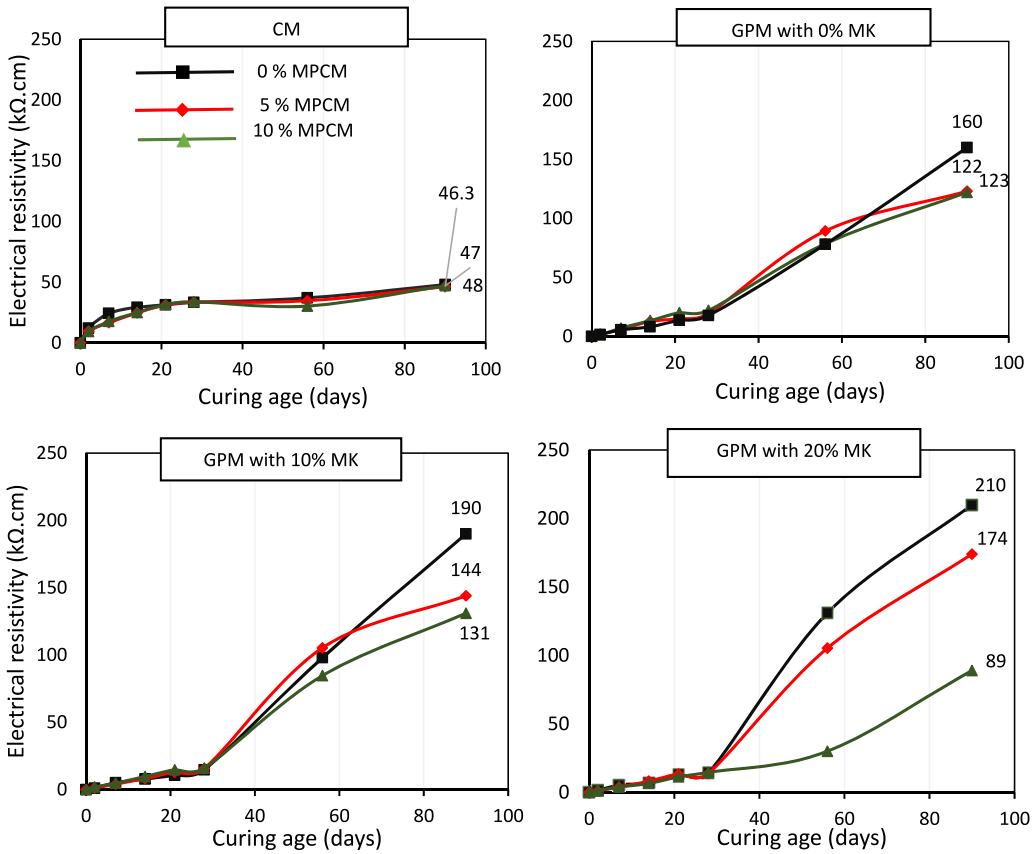

Fig. 7. Electrical resistivity as a function of curing time, A:(CM), B:(GPM with 0% MK); C:(GPM with 10% MK); D:(GPM with 20% MK).

Table 4
Relationship between concrete resistivity and corrosion rate [61].

Corrosion risk	Resistivity value (kΩ.cm)
High	<5
Moderate	5–10
Low	10–20
Negligible	>20

Friedel's salt $Ca_2Al(OH)_6Cl{\cdot}2H_2O$ (hydrated calcium chloroaluminate). This explains the increase in the amount of bound chloride as the chloride concentration of the initial solution increases.

Binding capacity of GPM (with 100% GBFS and 0% MPCM) at a free chloride concentration of 1 mol/l is 24.9 mg/g. This value is within the range reported for geopolymers in the studies by Fu et al. [65] and Zhang et al. [66] as presented in Fig. 8 (C). However, GPM shows a sharp increase in the amount of bound chloride compared to CM. CM has a chloride binding capacity of 11.7 mg/g, which is lower than that of GPM (with 100% GBFS and 0% MPCM). This is confirmed by Fu et al. [65] and Gunasekara et al. [68] who have shown that geopolymers can fix a higher amount of chloride than cement-based materials. Furthermore, Fu et al. [65] report a 100% increase in the amount of bound Cl^- for geopolymer pastes in comparison with OPC. This binding mechanism can be attributed to two combined actions: free chloride physical binding in CASH and NASH gels [66] and chemical binding due to chloride reactions with alumina and calcium oxide in undissolved GBFS and MK grains, forming Friedel's salt [54].

GPM with 100% GBFS with and without MPCM has maximum chloride binding capacity. This is due to the fact that CASH gels have a positively charged surface in alkaline solutions. A more positively charged surface is more likely expected to result in a higher OH^- and Cl^- adsorption [66]. In contrast, MK addition results in a decrease in chloride adsorption due to the formation of NASH gel. This is pointed out by Fu et al. [65]. From their DRX analysis of MK-based geopolymers, the authors observed that the mineralogical phases change slightly after chloride contamination. They explain that chloride ions are likely to be physically bound to the surface of NASH gels, which may account for the smaller decrease in Cl^- binding after MIK addition.

MPCM addition also increases the binding capacity of all the mortars tested. This effect is probably due to MPCM physical binding (adsorption) with the plastic walls and possibly related to their agglomeration as shown in Fig. 5. Indeed, due to the small size of MPCM

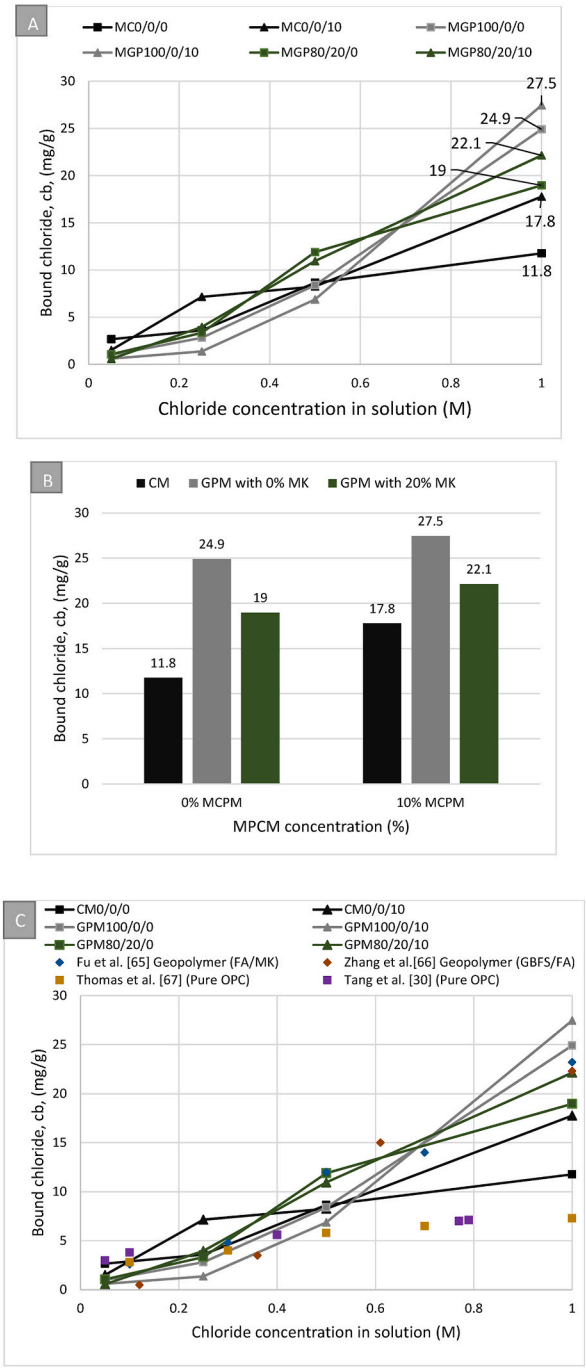

Fig. 8. (A): Chloride binding isotherms as a function of free chloride; (B): Chloride binding isotherms at 1 mol/l chloride as a function of MPCM concentration for: $CM_{0/0/0}$; $CM_{0/0/10}$; $GPM_{100/0/0}$; $GPM_{100/0/10}$; $GPM_{80/20/0}$; $GPM_{80/20/10}$. (C): Chloride binding isotherms of CM and GPM compared with literature studies by Fu et al. [65], Zhang et al. [66], Thomas et al. [67] and Tang et al. [30] with a range of chloride concentration in the solution between 0 and 1.0 M.

(size between 6.19 and 38.22 μm) compared to that of sand materials, MPCM agglomeration can trap chloride through the matrix.

3.4.2. Stationary state migration test 'D_{ss}'

Fig. 9 presents the stationary-state chloride migration measurements of the samples after 28 days of curing. Fig. 9 (A) displays cumulative chloride concentration results measured in the downstream compartment versus time. Fig. 9 (B) shows the stationary-state chloride migration coefficient D_{ss}.

CM with 0% MPCM reveals a significantly lower cumulative chloride concentration rate than GPM with 100% GBFS and 0% MPCM.

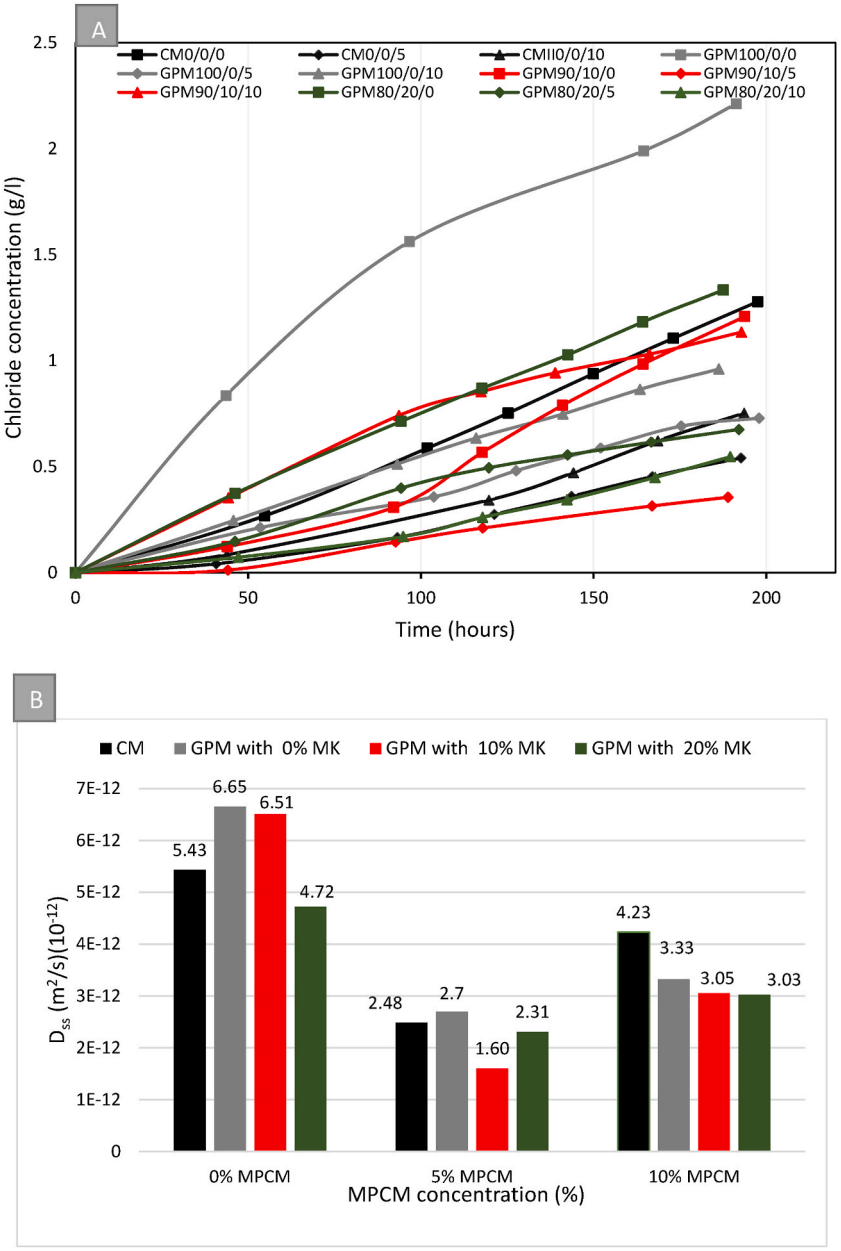

Fig. 9. Stationary-state chloride migration measurement: (A) Cumulative chloride concentration vs. time, (B) Stationary state migration coefficient 'D_{ss}'.

Typically, in this type of test, cement-based materials are affected by chloride adsorption on the capillary pore walls. This adsorption is the result of the reactions of chlorides with aluminates present in the cement matrix. These reactions lead to the hydration of C_3A and C_4AF and to the formation of Friedel's salt, which reduces chloride concentration rate [30]. On the other hand, the physical binding, whose chloride adsorption occurs on the CSH hydration gel products, delays chloride penetration of [69]. As discussed in Section 3.4.1, these physical and chemical bindings are observed in GPM. Fig. 9 (A) shows that GPM with 10 and 20% MK has a lower cumulative chloride concentration rate than GPM with 100% GBFS, and hence a lower migration coefficient. Furthermore, the chloride isotherm binding measurements reveal the opposite, indicating that MK addition reduces binding. Indeed, mechanisms influencing chloride penetration into geopolymers remains poorly understood [53]. One explanation is that the NASH gel formed after MK addition of is more resistant to the drying temperature than the CASH gel formed by GBFS activation [20]. This may also further reduce pore interconnection compared with mortars with 100% GBFS. Moreover, it has been proved that MK addition reduces the GPM critical diameter "dcr" and the total porosity measured by MIP, thus reducing pore interconnection [55]. MK addition furthermore increases electrical resistivity. As discussed above, a material containing a smaller number of interconnected pores with a more tortuous path will block the passage of ions through the porous structure. Polder et al. [70] report that low concrete resistivity is correlated with a

rapid chloride penetration and a high corrosion rate. Besides, Bernal et al. [13] and Mehta et al. [71] have pointed out that the coexistence of CASH and NASH gels to form the CNASH gel is effective in preventing chloride penetration in geopolymer-based materials. All these reasons may account for the reduction of chloride ion penetration in GPM after MK addition.

MPCM addition of also leads to a decrease in penetration of chloride ions in all the mortars studied. As explained in Section 3.1, this may be due to the increase in tortuosity caused by MPCM agglomeration, which reduces critical pore diameter. Indeed, increased tortuosity plays a very important role in transport properties of building materials, in particular chloride diffusion coefficient. Bi et al. [72] point out that this behavior may be explained by the filling of PCM pores in the mortars, which can then block the mortar capillary channels and increase their tortuosity, thus preventing water from penetrating mortars.

Caré [73] highlights that tortuosity depends on the aggregate volume fraction and is characterized by the enhancement of the path for diffusive species due to the tortuous pore network caused by the aggregates. The authors come to the conclusion that the aggregates modify cement paste pore structure and transport properties of sodium chloride ions. Another explanation could be the non-porous nature of MPCM (non-permeable) compared with the porous nature of sand, which can block the chloride ion ingress. Finally, the large amount of Cl-that is bound by MPCMs (Section 3.4.1) may be another reason for this reduction in chloride ion penetration.

Fig. 10 shows a comparison between the results obtained by Bernal et al. [13], Junior el al [74]. and Caré [73] for stationary-state chloride migration coefficient D_{ss} and total water porosity. Fig. 10 shows the D_{ss} coefficient increases with porosity. Indeed, porosity is the main parameter affecting chloride diffusivity [73]. The results obtained by Bernal et al. [13] show that the D_{ss} coefficient is relatively low, which is associated with low porosity. This is generally related to the low E/binder ratio chosen here, in comparison with the ratios used in the studies presented in Fig. 10. According to Yang et al. [75], the traditional classification of concrete pores has two categories: gel pores (<10 nm), which are associated with the formation of hydration products, and capillary pores (10-10,000 nm). Capillary pores are the residual voids originally filled by mixing water. When hydration begins, the capillary pore space is completely percolated. These pores are much larger than those found in C–S–H gel. Therefore, they dominate chloride ion transport processes. This explains why the amount of void (porosity) caused by water evaporation during curing is the most significant effect of the correlation shown in Fig. 10.

3.4.3. *Non-stationary state migration test 'D_{nss}'*

Fig. 12 shows the measurements of the D_{nss} migration coefficient in non-stationary state conditions after 28 days of curing for all the mortars tested in this study. On completion of the measurement process, silver nitrate ($AgNO_3$) is applied to the fractured samples to determine chloride penetration depth, which is called "X_d". As shown in Equation (8) and Fig. 11, silver nitrate reacts with chloride and hydroxyl ions to form white AgCl and dark brown Ag_2O. Fig. 11 displays chloride penetration depth (white color) determined for CM and GPM with 10% MPCM.

$$\begin{aligned} &Ag^+ + Cl^- \rightarrow AgCl \downarrow (\text{silver} - \text{white}) \\ &Ag^+ + OH \rightarrow AgOH \rightarrow Ag_2O \downarrow (\text{brown}) \end{aligned} \tag{8}$$

D_{nss} chloride migration coefficient values are significantly higher for GPM than for CM. This may be related to the difference in pore structure of the two types of mortar presented in Section 3.1, where GPM exhibits very large pore diameters compared with CM. Besides, migration testing performed in non-stationary state conditions under an electric field is considered to be a very fast test. Moreover, in the presence of a sufficiently large electric field, as is the case here, the diffusion term of the equation is negligible compared to the electric migration term [76]. For this reason, Samson et al. [77] and Baroghel et al. [78] consider that chloride binding

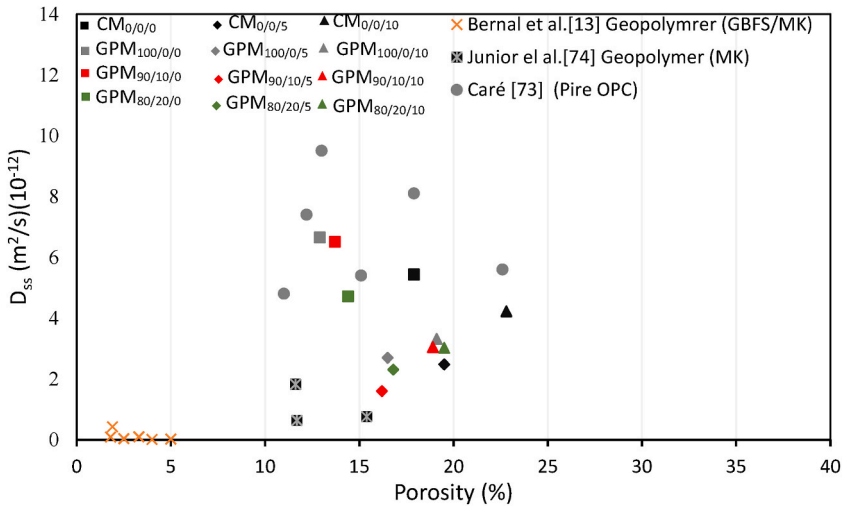

Fig. 10. Correlation between stationary -state chloride migration coefficient Dss and total water porosity/a comparison with studies reported by Bernal et al. [13] Junior el al [74]. and Caré [73].

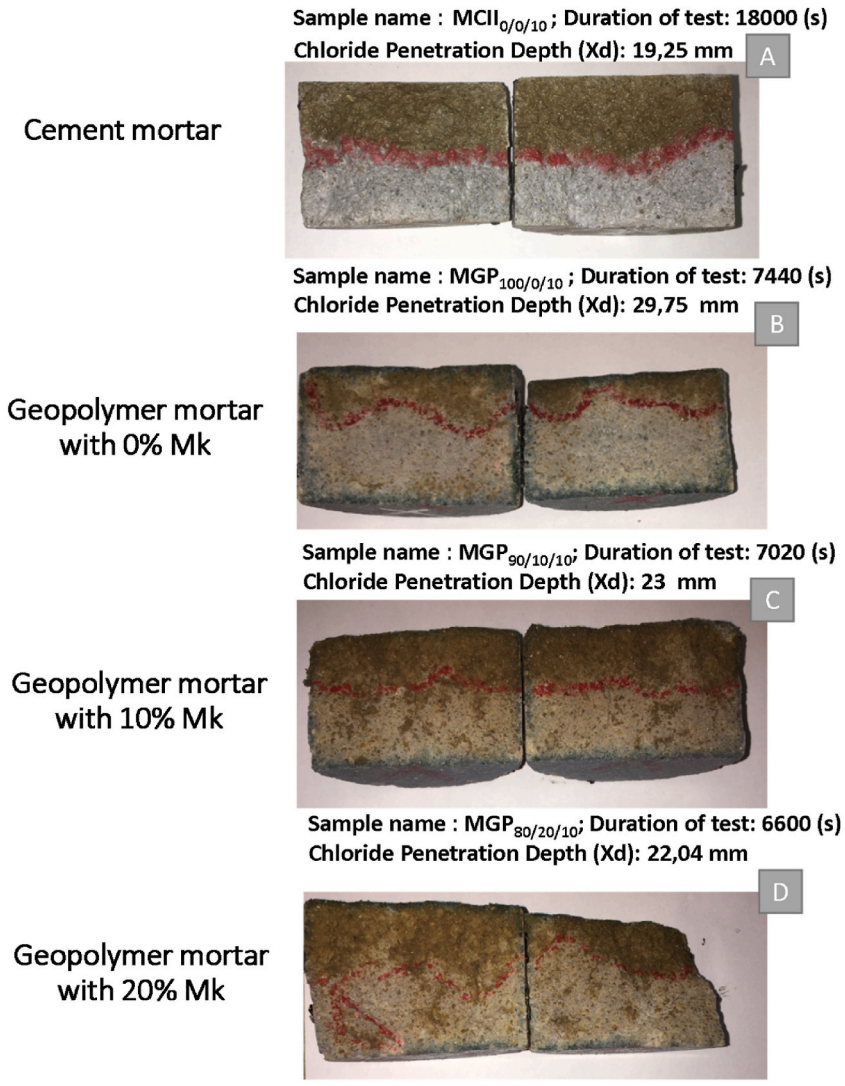

Fig. 11. Penetration depth of chloride ions "X_d" by application of AgNO3 on cement and GPM with 10% MPCM after 28 days of curing: (A) $MCII_{0/0/10}$; (B) $GPM_{100/0/10}$; (C) $GPM_{90/10/10}$; (D) $GPM_{80/20/10}$.

can be neglected in the tests by assuming, notably, that solutions are very diluted and that chlorides are the only species in the pore solution [29]. Baroghel et al. [78] also point out that, in this test, the ion transport rate through the porous structure is very high and contact time short. Therefore, assuming instantaneous chloride binding is not valid [78]. This may explain why ion transport velocity is very high in GPMs, due to their porous structure compared with CM. In this context, it is important to calculate the D_{nss} coefficient directly from the measured D_{ss} values.

In order to calculate the "D_{nss}" (m^2/s) coefficient from the natural diffusion under certain assumptions, a relationship with the "D_{ss}" (m^2/s) coefficient [29] is established as:

$$D_{nss} = \frac{D_{ss}}{\left(\varphi + \rho . \frac{dc_b}{dc_f}\right)} \tag{9}$$

where " φ " is the total porosity of the material (%), c_f is the concentration of the interstitial solution in free chlorides (kg of chloride/m^3 of solution), $c_{b\ is}$ the mass of bound chlorides (kg of chloride/kg of concrete), ρ is the apparent density of the dry material (kg/m^3), and $K_d = \frac{dc_b}{dc_f}$ is the so-called binding capacity (slope of the chloride binding "isotherm") implicitly assumed to be constant. Tang et al. [76] also confirm the existence of a linear relationship, similar to Equation (9), between the measured coefficients D_{ss} and D_{nss}, by applying an electric field, (migration) for cementious concrete. This shows that the coefficient D_{ss} can be deduced from the effective chloride migration coefficient D_{nss} directly determined using a short migration test. It is assumed that no binding occurs ($K_d = 0$) during this short migration test [29]. The relationship for calculating D_{nss} is given in Equation (10) [29] in the form:

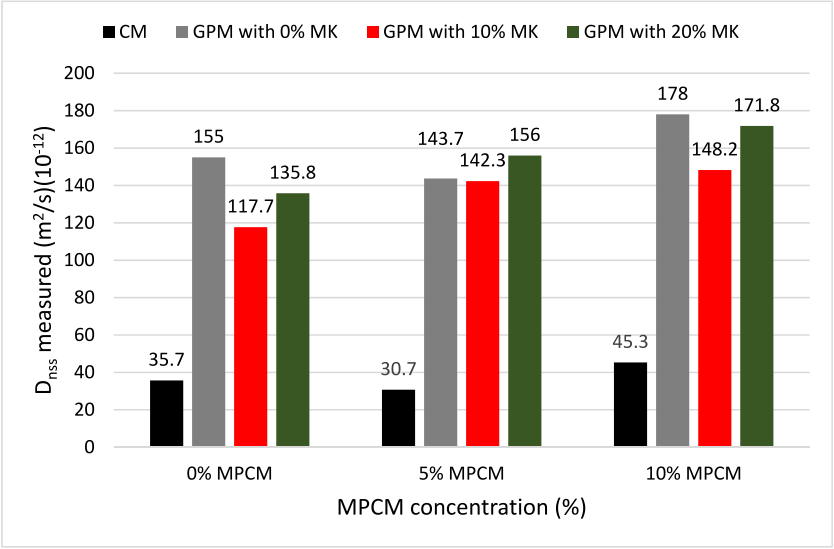

Fig. 12. Chloride migration coefficient in non-stationary state 'D_{nss}'.

$$D_{nss} = \frac{D_{ss}}{\varphi} \tag{10}$$

Fig. 13 shows the D_{nss} values calculated from Equation (10) and a correlation between D_{ss} and D_{nss} calculated from Equations (9) and (10) and D_{nss} measurements. It should be noted that D_{nss} values for CM are consistent with measured values (good correlation). The good agreement between D_{nss} calculated using Equation (10) and measured D_{nss} for CM confirms that chloride binding in migration tests is very limited and that assuming $C_b = 0$ is acceptable in most cases. Furthermore, Baroghel et al. [79] point out that the determination of the average chloride penetration depth 'X_d' using the $AgNO_3$ spray test is sufficiently accurate, with confirms the reliability of this method.

Compared to the measured and calculated 'D_{nss}' values, GPM exhibits very low 'D_{ss}' coefficient values. When comparing both methods (stationary and non-stationary), a factor between 28 and 30 is obtained for GPM. Ismail et al. [54] have also determined a factor of 100 for geopolymer concrete materials.

This can be accounted for by two hypotheses.

- The long duration of the stationary migration test, which may affect chloride diffusion rate in the geopolymer matrix at the time of the test. This can change pore structure [54]. Ismail et al. [54] point out that the increase in maturity of the binding phases with time, could delay chloride penetration through the geopolymer pore network. This is not the case in the non-stationary state chloride migration method. Chindaprasirt et al. [80] report that the geopolymer chemical composition influences chloride penetration resistance more than its porous structure. Despite high porosity, geopolymer chemical composition can play an important role in controlling chloride penetration in stationary state conditions compared with non-stationary state ones [80]. This is confirmed by the high chloride ion binding capacity of GPM compared with CM discussed in Section 3.4.1.
- Measuring D_{nss} in accordance with standard XP-P18-462 similar to standard NT BUILD-492 [45] may not be appropriate for GP materials. We can question the concentration of $AgNO_3$, which would react for very low chloride concentration, used for these materials. The calculation of D_{nss} requires the free chloride concentration limit value ($mol.l^{-1}$), at which the colorimetric test indicates a change in color. This value, which is assumed to be 0.070 mol l^{-1} by Tang et al. [46], is determined for Portland cements and not for GPM. This value would probably need to be reconsidered for geopolymer-based materials.

4. Conclusion

This paper investigates the effects of MPCM incorporation on chloride ion transport properties of reference geopolymer and cement-based mortars. Stationary and non-stationary methods used to assess chloride migration are examined. The impact CASH and NASH gel coexistence on chloride ion transport properties is also studied.

Based on the results obtained, the following conclusions are drawn.

I) MPCM addition increases total porosity, water absorption by capillary, decreases electrical resistivity, and does not affect pore size.

II) In spite of the increase in the total porosity observed, critical diameter measurements show that MPCM addition decreases pore connectivity. CASH and NASH gel coexistence demonstrates the densification and refinement of the geopolymer microstructure.

III) MPCM addition increases chloride binding capacity of both types of mortar (geopolymer-based and cement-based). This suggests that this finding may arise from a physical binding to MPCM walls. Compared with cement-based mortars, GPMs have very

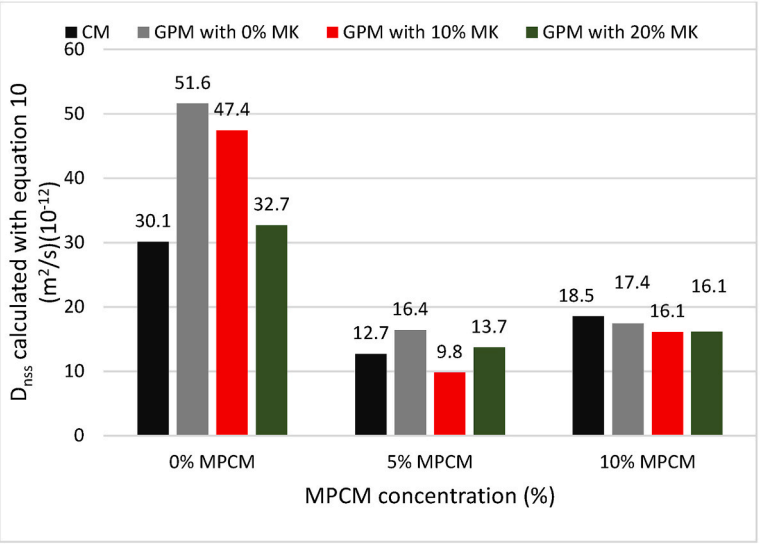

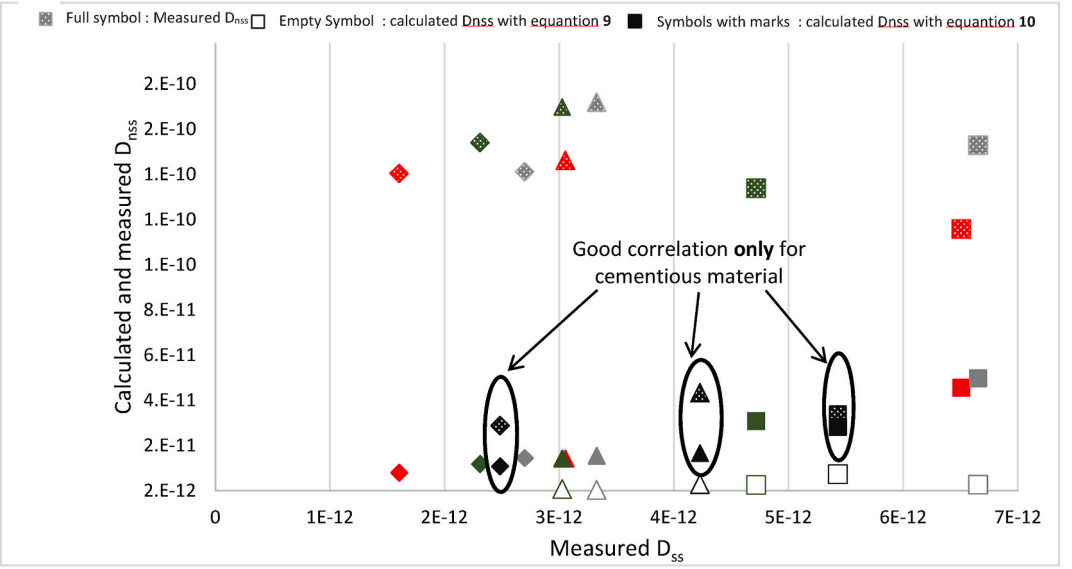

Fig. 13. (A): Calculated D_{nss}; (B): Correlation between D_{ss} and D_{nss} calculated from Equations (9) and (10) and D_{nss} measurements.

high chloride binding capacity. This is generally attributed to physical binding to the CASH and NASH gel walls, on the one hand, and to chemical binding where the aluminosilicate precursors react with Cl^- to form Friedel's salt, on the other hand.

IV) When comparing stationary and non-stationary chloride migration measurements, it is important to note that, during stationary testing, chloride chemistry and transport mechanisms in geopolymers are affected by the main geopolymerization derived products, like CASH and NASH gels. Moreover, the time required for the binding phases to mature delays chloride penetration. This is not the case with the non-stationary migration method.

V) D_{nss} measurement using the non-stationary-state chloride ion migration method underlines the technical limitations of GPM characterization in comparison with CM.

With a view to long-term development of MPCM-geopolymers, gas permeability and drying shrinkage should be determined, and sodium chloride binding and pore solution should be further investigated.

Credit authorship contribution statement

Bouha EL MOUSTAPHA: Conceptualization, Methodology, Investigation, Writing - original draft. Stéphanie BONNET: Validation,

Resources, Visualization, Supervision, review & editing. Abdelhafid KHELIDJ: Validation, Resources, Visualization, Supervision, review & editing. Nicolas MARANZANA: Validation, review & editing. Daniel FROELICH: Validation, review & editing, Supervision. Isselmou AHMEDOU BABAH: review & editing, Supervision. Abderahmane KHALIFA: Funding.

Declaration of competing interest

The authors declare that they have no known competing financial interests or personal relationships that could have appeared to influence the work reported in this paper.

Data availability

No data was used for the research described in the article.

Acknowledgements

The experimental study has been carried out at the Institute of Research in Civil and Mechanical Engineering - Nantes Université, Ecole Centrale Nantes,CNRS UMR 6183, Saint Nazaire, France. . In this regard, we would like to thank the head of the Institute of Research in Civil and Mechanical Engineering and the head of the Magma laboratory for their support in the realization of this study.

References

[1] Energy efficiency – topics, IEA, https://www.iea.org/topics/energy-efficiency (consulté le 22 mars 2022).
[2] N. Llantoy, M. Chàfer, , et al.L.F. Cabeza, A comparative life cycle assessment (LCA) of different insulation materials for buildings in the continental Mediterranean climate, oct, Energy Build. 225 (2020), 110323, https://doi.org/10.1016/j.enbuild.2020.110323.
[3] A.M. Thiele, G. Sant, , et al.L. Pilon, Diurnal Thermal Analysis of Microencapsulated PCM-Concrete Composite Walls, vol. 93, Energy Conversion and Management, mars 2015, pp. 215–227, https://doi.org/10.1016/j.enconman.2014.12.078.
[4] P.-C. Aıtcin, Cements of yesterday and today: concrete of tomorrow, sept, Cement Concr. Res. 30 (9) (2000) 1349–1359, https://doi.org/10.1016/S0008-8846(00)00365-3.
[5] M. Ren, X. Wen, X. Gao, , et al.Y. Liu, Thermal and mechanical properties of ultra-high performance concrete incorporated with microencapsulated phase change material, Construct. Build. Mater. 273 (mars 2021), 121714, https://doi.org/10.1016/j.conbuildmat.2020.121714.
[6] P.K. Singh Rathore, S.K. Shukla, , et al.N.K. Gupta, Potential of microencapsulated PCM for energy savings in buildings: a critical review, Sustain. Cities Soc. 53 (févr. 2020), 101884, https://doi.org/10.1016/j.scs.2019.101884.
[7] S. Drissi, T.-C. Ling, K.H. Mo, , et al.A. Eddhahak, A review of microencapsulated and composite phase change materials: alteration of strength and thermal properties of cement-based materials, août, Renew. Sustain. Energy Rev. 110 (2019) 467–484, https://doi.org/10.1016/j.rser.2019.04.072.
[8] K.-H. Yang, Y.-B. Jung, M.-S. Cho, , et al.S.-H. Tae, Effect of supplementary cementitious materials on reduction of CO2 emissions from concrete, sept, J. Clean. Prod. 103 (2015) 774–783, https://doi.org/10.1016/j.jclepro.2014.03.018.
[9] A. Palomo, M.W. Grutzeck, , et al.M.T. Blanco, Alkali-activated fly ashes: a cement for the future, août, Cement Concr. Res. 29 (8) (1999) 1323–1329, https://doi.org/10.1016/S0008-8846(98)00243-9.
[10] J. Davidovits, Geopolymer Cement a Review 2013, janv, 2013, pp. 1–11.
[11] F.N. Okoye, S. Prakash, , et al.N.B. Singh, Durability of fly ash based geopolymer concrete in the presence of silica fume, J. Clean. Prod. 149 (2017) 1062–1067, https://doi.org/10.1016/j.jclepro.2017.02.176, avr.
[12] W.G. Valencia Saavedra, , et al.R. Mejía de Gutiérrez, Performance of geopolymer concrete composed of fly ash after exposure to elevated temperatures, nov, Construct. Build. Mater. 154 (2017) 229–235, https://doi.org/10.1016/j.conbuildmat.2017.07.208.
[13] S.A. Bernal, R. Mejía de Gutiérrez, , et al.J.L. Provis, Engineering and durability properties of concretes based on alkali-activated granulated blast furnace slag/metakaolin blends, août, Construct. Build. Mater. 33 (2012) 99–108, https://doi.org/10.1016/j.conbuildmat.2012.01.017.
[14] R. Shadnia, L. Zhang, , et al.P. Li, Experimental study of geopolymer mortar with incorporated PCM, juin, Construct. Build. Mater. 84 (2015) 95–102, https://doi.org/10.1016/j.conbuildmat.2015.03.066.
[15] V.D. Cao, et al., Thermal analysis of geopolymer concrete walls containing microencapsulated phase change materials for building applications, janv, Sol. Energy 178 (2019) 295–307, https://doi.org/10.1016/j.solener.2018.12.039.
[16] B. El Moustapha, et al., Compensation of the negative effects of micro-encapsulated phase change materials by incorporating metakaolin in geopolymers based on blast furnace slag, Construct. Build. Mater. 314 (2022), 125556, https://doi.org/10.1016/j.conbuildmat.2021.125556 janv.
[17] Y. Fang, M.R. Ahmad, J.-C. Lao, L.-P. Qian, , et al.J.-G. Dai, Development of artificial geopolymer aggregates with thermal energy storage capacity, Cement Concr. Compos. 135 (janv. 2023), 104834, https://doi.org/10.1016/j.cemconcomp.2022.104834.
[18] M. Muraleedharan, , et al.Y. Nadir, Geopolymer mortar integrated with phase change materials for improvement of thermal efficiency in buildings: a review, janv, Mater. Today: Proc. 44 (2021) 878–885, https://doi.org/10.1016/j.matpr.2020.10.791.
[19] Climat, Vers un dérèglement géopolitique. https://www.senat.fr/rap/r15-014/r15-0143.html (consulté le 22 mars 2022).
[20] A. Neville, Chloride attack of reinforced concrete: an overview, Mater. Struct. 28 (2) (1995) 63–70, https://doi.org/10.1007/BF02473172, mars.
[21] K. Vance, M. Aguayo, A. Dakhane, D. Ravikumar, J. Jain, , et al.N. Neithalath, Microstructural, mechanical, and durability related similarities in concretes based on OPC and alkali-activated slag binders, Int J Concr Struct Mater 8 (4) (2014) 289–299, https://doi.org/10.1007/s40069-014-0082-3, déc.
[22] D. Ravikumar, , et al.N. Neithalath, An electrical impedance investigation into the chloride ion transport resistance of alkali silicate powder activated slag concretes, nov, Cement Concr. Compos. 44 (2013) 58–68, https://doi.org/10.1016/j.cemconcomp.2013.06.002.
[23] K.-S. Huang, , et al.C.-C. Yang, Using RCPT determine the migration coefficient to assess the durability of concrete, avr, Construct. Build. Mater. 167 (2018) 822–830, https://doi.org/10.1016/j.conbuildmat.2018.02.109.
[24] R.R. Lloyd, J.L. Provis, , et al.J.S.J. van Deventer, Pore solution composition and alkali diffusion in inorganic polymer cement, sept, Cement Concr. Res. 40 (9) (2010) 1386–1392, https://doi.org/10.1016/j.cemconres.2010.04.008.
[25] S.A. Bernal, , et al.J.L. Provis, Durability of alkali-activated materials: progress and perspectives, J. Am. Ceram. Soc. 97 (4) (2014) 997–1008, https://doi.org/10.1111/jace.12831.
[26] C. Andrade, Calculation of chloride diffusion coefficients in concrete from ionic migration measurements, mai, Cement Concr. Res. 23 (3) (1993) 724–742, https://doi.org/10.1016/0008-8846(93)90023-3.
[27] O. Truc, J.P. Ollivier, , et al.M. Carcassès, A new way for determining the chloride diffusion coefficient in concrete from steady state migration test, févr, Cement Concr. Res. 30 (2) (2000) 217–226, https://doi.org/10.1016/S0008-8846(99)00232-X.
[28] T. Luping, , et al.L.-O. Nilsson, Chloride diffusivity in high strength concrete at different ages, NORDIC CONCRETE RESEARCH. PUBLICA*TION NO 11*, févr. 1992, Consulté le: 23 mars 2022. [En ligne]. Disponible sur: https://trid.trb.org/view/376238.

[29] V. Baroghel-Bouny, K. Kinomura, M. Thiery, , et al.S. Moscardelli, Easy assessment of durability indicators for service life prediction or quality control of concretes with high volumes of supplementary cementitious materials, sept, Cement Concr. Compos. 33 (8) (2011) 832–847, https://doi.org/10.1016/j.cemconcomp.2011.04.007.
[30] T. Luping, , et al.L.-O. Nilsson, Chloride binding capacity and binding isotherms of OPC pastes and mortars, mars, Cement Concr. Res. 23 (2) (1993) 247–253, https://doi.org/10.1016/0008-8846(93)90089-R.
[31] P.S. Mangat, , et al.O.O. Ojedokun, Free and bound chloride relationships affecting reinforcement cover in alkali activated concrete, Cement Concr. Compos. 112 (sept. 2020), 103692, https://doi.org/10.1016/j.cemconcomp.2020.103692.
[32] B. Martın-Perez, H. Zibara, R.D. Hooton, , et al.M.D.A. Thomas, A study of the effect of chloride binding on service life predictions, août, Cement Concr. Res. 30 (8) (2000) 1215–1223, https://doi.org/10.1016/S0008-8846(00)00339-2.
[33] A. Noushini, , et al.A. Castel, The effect of heat-curing on transport properties of low-calcium fly ash-based geopolymer concrete, juin, Construct. Build. Mater. 112 (2016) 464–477, https://doi.org/10.1016/j.conbuildmat.2016.02.210.
[34] STANDARD, N. F. EN 197-1, Cement-Part1: Composition, Specifications and Compliance Criteria for Common Cements, 2012.
[35] A. Hasnaoui, E. Ghorbel, , et al.G. Wardeh, Optimization approach of granulated blast furnace slag and metakaolin based geopolymer mortars, févr, Construct. Build. Mater. 198 (2019) 10–26, https://doi.org/10.1016/j.conbuildmat.2018.11.251.
[36] S. Pilehvar, et al., Physical and mechanical properties of fly ash and slag geopolymer concrete containing different types of micro-encapsulated phase change materials, juin, Construct. Build. Mater. 173 (2018) 28–39, https://doi.org/10.1016/j.conbuildmat.2018.04.016.
[37] « EN 196-1, Methods of Testing Cement- Part 1: Determination of Strength, European committee for standardization, 2016.
[38] S. Pilehvar, et al., Effect of freeze-thaw cycles on the mechanical behavior of geopolymer concrete and Portland cement concrete containing micro-encapsulated phase change materials, Construct. Build. Mater. 200 (2019) 94–103, https://doi.org/10.1016/j.conbuildmat.2018.12.057, mars.
[39] NF P 18-459, Concrete – Testing Hardened Concrete-Testing Porosity and Density, French Association for Standardization AFNOR, 2010.
[40] H. Giesche, Mercury porosimetry: a general (practical) overview, Part. Part. Syst. Char. 23 (1) (2006) 9–19, https://doi.org/10.1002/ppsc.200601009.
[41] NF EN 13057. Determination of Resistance of Capillary Absorption ».
[42] S. Bonnet, , et al.J.-P. Balayssac, Combination of the Wenner resistivimeter and Torrent permeameter methods for assessing carbonation depth and saturation level of concrete, nov, Construct. Build. Mater. 188 (2018) 1149–1165, https://doi.org/10.1016/j.conbuildmat.2018.07.151.
[43] NF XP P18-461, Test on Hardened Concrete: Accelerated Test of Chloride Ions in Steady State, Determination of the Effective Diffusion Coefficient of Chloride Ions, French Standard, France, 2012 (in French).
[44] NF XP P18-462, Test on Hardened Concrete: Accelerated Test of Chloride Ions in Non-steady State, Determination of the Apparent Diffusion Coefficient of Chloride Ions, French Standard, France, 2012 (in French).
[45] NORDTEST METHOD, NT Build 492. Concrete, Mortar and Cement-Based Repair Materials: Chloride Migration Coefficient from Non-steady-state Migration Experiments, 1999.
[46] L. Tang, Electrically accelerated methods for determining chloride diffusivity in concrete—current development, Mag. Concr. Res. 48 (176) (sept. 1996) 173–179, https://doi.org/10.1680/macr.1996.48.176.173.
[47] K.K. Aligizaki, Pore Structure of Cement-Based Materials: Testing, Interpretation and Requirements, CRC Press, London, 2014, https://doi.org/10.1201/9781482271959.
[48] P.H.R. Borges, N. Banthia, H.A. Alcamand, W.L. Vasconcelos, , et al.E.H.M. Nunes, Performance of blended metakaolin/blastfurnace slag alkali-activated mortars, août, Cement Concr. Compos. 71 (2016) 42–52, https://doi.org/10.1016/j.cemconcomp.2016.04.008.
[49] M. Yang, S.R. Paudel, , et al.E. Asa, Comparison of pore structure in alkali activated fly ash geopolymer and ordinary concrete due to alkali-silica reaction using micro-computed tomography, Construct. Build. Mater. 236 (mars 2020), 117524, https://doi.org/10.1016/j.conbuildmat.2019.117524.
[50] V.D. Cao, et al., Influence of microcapsule size and shell polarity on thermal and mechanical properties of thermoregulating geopolymer concrete for passive building applications, Energy Convers. Manag. 164 (mai 2018) 198–209, https://doi.org/10.1016/j.enconman.2018.02.076.
[51] M. Hunger, A.G. Entrop, I. Mandilaras, H.J.H. Brouwers, , et al.M. Founti, The behavior of self-compacting concrete containing micro-encapsulated Phase Change Materials, nov, Cement Concr. Compos. 31 (10) (2009) 731–743, https://doi.org/10.1016/j.cemconcomp.2009.08.002.
[52] F. Matalkah, T. Salem, M. Shaafaey, , et al.P. Soroushian, Drying shrinkage of alkali activated binders cured at room temperature, Construct. Build. Mater. 201 (2019) 563–570, https://doi.org/10.1016/j.conbuildmat.2018.12.223, mars.
[53] J. Zhang, C. Shi, Z. Zhang, , et al.Z. Ou, Durability of alkali-activated materials in aggressive environments: a review on recent studies, oct, Construct. Build. Mater. 152 (2017) 598–613, https://doi.org/10.1016/j.conbuildmat.2017.07.027.
[54] I. Ismail, et al., Influence of fly ash on the water and chloride permeability of alkali-activated slag mortars and concretes, nov, Construct. Build. Mater. 48 (2013) 1187–1201, https://doi.org/10.1016/j.conbuildmat.2013.07.106.
[55] P. Pipilikaki, , et al.M. Beazi-Katsioti, The assessment of porosity and pore size distribution of limestone Portland cement pastes, mai, Construct. Build. Mater. 23 (5) (2009) 1966–1970, https://doi.org/10.1016/j.conbuildmat.2008.08.028.
[56] Z. Wei, et al., The durability of cementitious composites containing microencapsulated phase change materials, août, Cement Concr. Compos. 81 (2017) 66–76, https://doi.org/10.1016/j.cemconcomp.2017.04.010.
[57] G.F. Huseien, J. Mirza, M. Ismail, S.K. Ghoshal, , et al.M.A.M. Ariffin, Effect of metakaolin replaced granulated blast furnace slag on fresh and early strength properties of geopolymer mortar, Ain Shams Eng. J. 9 (4) (2018) 1557–1566, https://doi.org/10.1016/j.asej.2016.11.011, déc.
[58] M. Ibrahim, M.A.M. Johari, M. Maslehuddin, , et al.M.K. Rahman, Influence of nano-SiO2 on the strength and microstructure of natural pozzolan based alkali activated concrete, juin, Construct. Build. Mater. 173 (2018) 573–585, https://doi.org/10.1016/j.conbuildmat.2018.04.051.
[59] A. Mobili, A. Belli, C. Giosuè, T. Bellezze, , et al.F. Tittarelli, Metakaolin and fly ash alkali-activated mortars compared with cementitious mortars at the same strength class, Cement Concr. Res. 88 (oct. 2016) 198–210, https://doi.org/10.1016/j.cemconres.2016.07.004.
[60] C. Gonilho Pereira, J. Castro-Gomes, , et al.L. Pereira de Oliveira, Influence of natural coarse aggregate size, mineralogy and water content on the permeability of structural concrete, févr, Construct. Build. Mater. 23 (2) (2009) 602–608, https://doi.org/10.1016/j.conbuildmat.2008.04.009.
[61] 222R-01 Protection of Metals in Concrete against Corrosion. nedatováno, 41.
[62] F.F. Zainal, et al., The electrical resistivity of geopolymer paste by using wenner four probe method, Key Eng. Mater. 660 (2015) 28–33. www.scientific.net/KEM.660.28.
[63] F. Ameri, P. Shoaei, S.A. Zareei, , et al.B. Behforouz, Geopolymers vs. alkali-activated materials (AAMs): a comparative study on durability, microstructure, and resistance to elevated temperatures of lightweight mortars, oct, Construct. Build. Mater. 222 (2019) 49–63, https://doi.org/10.1016/j.conbuildmat.2019.06.079.
[64] P. Rovnaník, I. Kusák, P. Bayer, P. Schmid, , et al.L. Fiala, Comparison of electrical and self-sensing properties of Portland cement and alkali-activated slag mortars, Cement Concr. Res. 118 (2019) 84–91, https://doi.org/10.1016/j.cemconres.2019.02.009, avr.
[65] C. Fu, H. Ye, K. Zhu, D. Fang, , et al.J. Zhou, Alkali cation effects on chloride binding of alkali-activated fly ash and metakaolin geopolymers, nov, Cement Concr. Compos. 114 (2020), 103721, https://doi.org/10.1016/j.cemconcomp.2020.103721.
[66] J. Zhang, C. Shi, , et al.Z. Zhang, Chloride binding of alkali-activated slag/fly ash cements, nov, Construct. Build. Mater. 226 (2019) 21–31, https://doi.org/10.1016/j.conbuildmat.2019.07.281.
[67] M.D.A. Thomas, R.D. Hooton, A. Scott, , et al.H. Zibara, The effect of supplementary cementitious materials on chloride binding in hardened cement paste, Cement Concr. Res. 42 (1) (2012) 1–7, https://doi.org/10.1016/j.cemconres.2011.01.001, janv.
[68] C. Gunasekara, D. Law, S. Bhuiyan, S. Setunge, , et al.L. Ward, Chloride induced corrosion in different fly ash based geopolymer concretes, mars, Construct. Build. Mater. 200 (2019) 502–513, https://doi.org/10.1016/j.conbuildmat.2018.12.168.
[69] H. Zibara, Binding of External Chlorides by Cement Pastes, Thesis, 2001. Consulté le: 31 mars 2022. [En ligne]. Disponible sur: https://tspace.library.utoronto.ca/handle/1807/15366.

[70] R. Polder, et al., Test methods for on site measurement of resistivity of concrete, Mater. Struct. 33 (10) (2000) 603–611, https://doi.org/10.1007/BF02480599, déc.
[71] A. Mehta, R. Siddique, T. Ozbakkaloglu, F. Uddin Ahmed Shaikh, , et al.R. Belarbi, Fly ash and ground granulated blast furnace slag-based alkali-activated concrete: mechanical, transport and microstructural properties, Construct. Build. Mater. 257 (oct. 2020), 119548, https://doi.org/10.1016/j.conbuildmat.2020.119548.
[72] L. Bi, G. Long, C. Ma, , et al.Y. Xie, Mechanical properties and water absorption of steam-cured mortar containing phase change composites, Construct. Build. Mater. 248 (2020), 118707, https://doi.org/10.1016/j.conbuildmat.2020.118707 juill.
[73] S. Caré, Influence of aggregates on chloride diffusion coefficient into mortar, juill, Cement Concr. Res. 33 (7) (2003) 1021–1028, https://doi.org/10.1016/S0008-8846(03)00009-7.
[74] N.S. Amorim Júnior, J.S. Andrade Neto, H.A. Santana, M.S. Cilla, , et al.D.V. Ribeiro, Durability and service life analysis of metakaolin-based geopolymer concretes with respect to chloride penetration using chloride migration test and corrosion potential, Construct. Build. Mater. 287 (juin 2021), 122970, https://doi.org/10.1016/j.conbuildmat.2021.122970.
[75] C.C. Yang, S.W. Cho, , et al.L.C. Wang, The relationship between pore structure and chloride diffusivity from ponding test in cement-based materials, Mater. Chem. Phys. 100 (2) (2006) 203–210, https://doi.org/10.1016/j.matchemphys.2005.12.032, déc.
[76] L. Tang, « Chloride Transport in Concrete-Measurement and Prediction », Chalmers University of Technology, Sweden, Doctor Thesis, 1996. Consulté le: 31 mars 2022. [En ligne]. Disponible sur: https://ci.nii.ac.jp/naid/10004008281/.
[77] E. Samson, J. Marchand, , et al.K.A. Snyder, Calculation of ionic diffusion coefficients on the basis of migration test results, Mater. Struct. 36 (3) (2003) 156–165, https://doi.org/10.1007/BF02479554, avr.
[78] V. Baroghel-Bouny, M. Thiéry, , et al.X. Wang, Modelling of isothermal coupled moisture–ion transport in cementitious materials, août, Cement Concr. Res. 41 (8) (2011) 828–841, https://doi.org/10.1016/j.cemconres.2011.04.001.
[79] V. Baroghel-Bouny, M. Thiery, F. Barberon, O. Coussy, , et al.G. Villain, Assessment of transport properties of cementitious materials, juin, Rev. Eur. Génie Civ. 11 (6) (2007) 671–696, https://doi.org/10.1080/17747120.2007.9692951.
[80] P. Chindaprasirt, , et al.W. Chalee, Effect of sodium hydroxide concentration on chloride penetration and steel corrosion of fly ash-based geopolymer concrete under marine site, juill, Construct. Build. Mater. 63 (2014) 303–310, https://doi.org/10.1016/j.conbuildmat.2014.04.010.